TEXAS CORN PRODUCERS BOARD

Performance and Consistency of Two Texas Bentonites as Atoxigenic Adsorbents of Aflatoxin and Fumonisin in Poultry Feed

ANNUAL REPORT: January 11, 2011

Principal Investigator: Dr. Joe B. Dixon
Emeritus Professor of Soil Clay Mineralogy
Department of Soil and Crop Sciences Texas A&M University
College Station TX 77843-2474
Phone: (979) 845-8323; FAX: (979) 845-0456
Email: j-dixon@tamu.edu

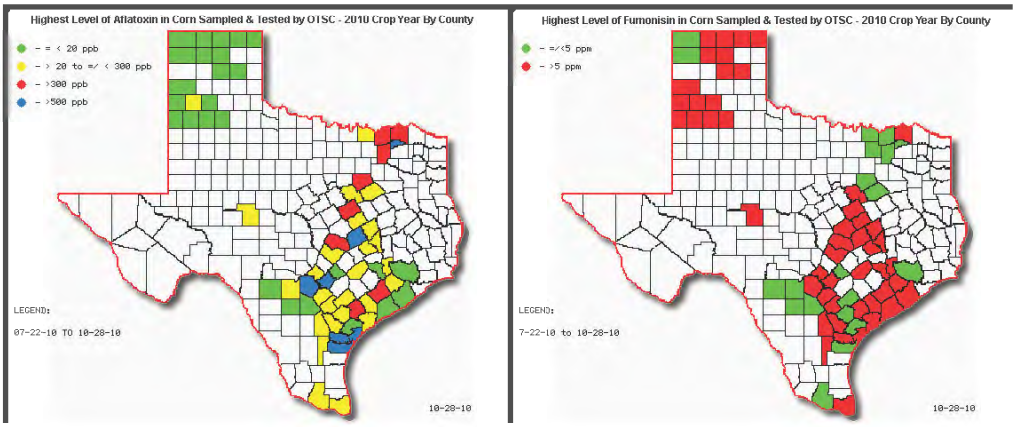

Figure1. Aflatoxin and Fumonisin levels in Texas corn for 2010 by Office of Texas State Chemist.

This project has progressed well through the selected stages of determining which bentonites were most effective adsorbents of aflatoxin from the USA and several other countries. The adsorption location of aflatoxin in smectite particles has been determined. Analytical methods for evaluating the adsorbent clays have been carefully chosen and published. Theoretical computation of aflatoxin bonding in smectite have been conducted and the theoretical findings support spectroscopic measurements. Results of this research have been published in several internationally respected scientific journals and others are in review or revision.

The best bentonite clay from Texas has been tested as feed amendment and limited animal performance tests demonstrated the clay is effective as an adsorbent of aflatoxin in chickens. These findings demonstrate that both domestic and international smectite adsorbents are available for controlling the effects of aflatoxin in animal feeds. Some ideas about improving efficacy of the clays in animal feeds have been proposed and will be tested in 2011.

During the year 2010 we participated in several meetings with grain producers, university agriculture faculty, and related disciplines from several states from central and southeastern United States and observed very little familiarity with smectite as an adsorbent of aflatoxin. There is clear concern for how to alleviate the losses from aflatoxin yet there is little evidence of how to accomplish a satisfactory solution. There is extensive concern for the unpredictability of aflatoxin in the field or in stored corn. Bentonite clay and its adsorption properties were rarely recognized in these discussions. These observations have led to the conclusion that a document based on the existing scientific data will be useful to grain producers, dealers, and animal feeders. We anticipate that when they are aware that bentonite is a reliable material to control aflatoxin they will improve their practices. Improved animal performance at low concentrations of the mycotoxin in feeds and grains for livestock will be an attractive option to apply to their own animals. Thus we propose to develop a book for use in the grain industry to help with management decisions in the grain industry. A draft introduction to that book is presented below:

Calcium smectite from bentonite to control aflatoxin in feeds.

Joe B. Dixon, Ana L. Barrientos Velázquez, Youjun Deng
Department of Soil and Crop Sciences Texas A&M University College Station, TX 77843-2474

Calcium bentonite adsorbents are rooted in the limit of one days travel by horse drawn wagon from clay mine to the woolen mill for cleaning wool in early English history. The adsorption of aflatoxin in bentonite clay is an important contribution to improved use of grains with low levels of aflatoxin in feed and food. The disciplined use of calcium bentonite can reduce the risk of cancer in animals and humans caused by aflatoxin. Aflatoxin research has demonstrated that 10 % of the bentonites tested are sufficiently effective to be used as feed amendment for animals. The recent need for expanded corn production for fuel alcohol increases the need for control of aflatoxin. These changes have increased research on the properties of smectite adsorbents and the molecular and structural factors that influence aflatoxin bonding in smectite. The best smectite adsorbents of aflatoxin have porosity produced by the calcium exchange ion and the clay interlayers are accessible to the mycotoxin. The bonding of aflatoxin occurs between smectite structural layers has been shown by x-ray diffraction measurements. Research results by instrumental measurements and theoretical calculations have confirmed that aflatoxin is bonded between calcium smectite structural layers. The bonding of aflatoxin between smectite layers persists during exchange of cations and water molecules around them. High resolution transmission electron microscope images illustrate the accessibility of calcium smectite to bond aflatoxin molecules among the best smectite adsorbents. Calcium smectites are the most effective adsorbents of aflatoxin attributed to the porous aggregates in contrast to exchangeable sodium smectites that tend to dry as thin sheets. The best smectite adsorbents of aflatoxin have lattice fringes and porous aggregates visible by high resolution transmission electron microscope. These findings indicate that the use of calcium bentonite to bind low levels of aflatoxin is sufficient for field testing in farm animals to improve their performance. This report is intended to communicate with

the public users of smectite adsorbents to expedite planning and practices that are economic and safe use of adsorbent and grain resources.

Progress with poultry investigations by Dr. Chris Bailey:

One of our goals is to seek more sensitive methods of evaluating aflatoxicosis in poultry. We think we may be able to detect responses in gene expression by renal and hepatic enzymes before overt signs of toxicosis occurs. Currently messenger RNA (mRNA) has been extracted from liver tissue samples of birds fed various levels of aflatoxin contaminated feed ranging from 0 to 2500 ppb. The samples of mRNA are scheduled to be copied into cDNA this week (03 January – 07 January). After cDNA synthesis our next step will be to analyze the samples using RT-PCR with primers associated with cytochrome P genes (CYP1A1), which are up-regulated in response to aflatoxin exposure. We hope to see up-regulation of the CYP1A1 gene at aflatoxin concentrations lower than those necessary to achieve significant weight loss. A significant CYP1A1 response at less than 1000 ppb would be a good measure of success.

Our Poultry rearing room was unofficially cleared for BL-1 in vivo poultry research on December 23rd, 2010. I am still waiting for the official letter of approval. We are growing our aflatoxin parasiticus cultures this week and will begin inoculating the DDGS either Friday of this week or early next week. We hope to have about 50 lbs of aflatoxin contaminated DDGS within 2 weeks. Our goal is at least 6,000 ppb aflatoxin. We have obtained enough clean DDGS (250 lbs) to perform a 3-week poultry grow-out trial with and without the bentonite clays. We will blend the contaminated DDGS with clean DDGS and corn to obtain several dietary concentrations ranging from 0 to ~ 2,000 ppb aflatoxin. At this point we plan on also incorporating the 800 ppb corn we have left over from the previous experiment (river bottom corn). There will be clean corn controls as well. I don't foresee any more holdups and we should be able to schedule the beginning of the poultry grow-out trial around the 1st of February.

Fumonisin B1 adsorbtion results in smectite by Dr. M.G. Tenorio Arvide:

The mycotoxicosis is an ignored global health issue and sits at the interface of agriculture, and economic problems. One of the most relevant mycotoxins is produced by the fungus Fusarium moniliform and proliferatum and it is called fumonisin B1, which constitutes about 70% of total fumonisin content found in naturally contaminated foods and feed. Also, the mycotoxin is a carcinogen to humans and animals. One of the detoxification methods includes inorganic adsorbent materials; especially smectite has been shown to give good results in aflatoxin sorption. We evaluated the efficacy of smectite in fumonisin B1adsorption under different conditions. A benonite clay from Gonzales TX was used in the fumonisin adsorbtion study. The x-ray diffraction measurements suggested interlayer adsorption of fumonisin B1 in smectite. Unlike the starting smectite itself, the fumonison-adsorbed smectite had a higher basal spacing at room humidity and did not collapse to 1.0~nm at 0% humidity with nitrogen purge. Fourier transform infrared (FTIR) spectroscopy results suggested that the interlayer adsorption decreased with increasing pH from 3 to 7. After washing two times with water, the in infrared

bands of the low pH samples remained, indicating the stability of the adsorbed fumonisin B1, especially at pH 3. These results suggested that it is possible to use the same smectite to adsorb aflatoxin and fumonisin.

Applied Clay Science 50 (2010) 92–98

Contents lists available at ScienceDirect

Applied Clay Science

journal homepage: www.elsevier.com/locate/clay

Bonding mechanisms between aflatoxin B_1 and smectite

Youjun Deng [a,*], Ana Luisa Barrientos Velázquez [a], Ferenc Billes [b], Joe B. Dixon [a]

[a] Department of Soil and Crop Sciences, Texas A&M University College Station, TX 77843-2474, United States
[b] Department of Physical Chemistry and Material Science, Budapest University of Technology and Economics, H-1521 Budapest, Budafoki út 8., Hungary

ARTICLE INFO

Article history:
Received 15 March 2010
Received in revised form 23 June 2010
Accepted 10 July 2010
Available online 24 July 2010

Keywords:
Aflatoxin B_1
Smectite
Ion-dipole interaction
H-bonding
Infrared

ABSTRACT

Bentonites were used in aflatoxin-contaminated feeds and diets to reduce bioavailability of the mycotoxin. The objectives of this study were to test accessibility of smectite interlayer space to aflatoxin adsorption and to investigate bonding mechanisms between adsorbed aflatoxin B_1 molecules and smectite. The aflatoxin–smectite complex had a basal spacing greater than 1.2 nm up to 400 °C, which suggests interlayer aflatoxin adsorption. The in-phase carbonyl-stretching band shifted from 1736 cm^{-1} for monovalent cation (K or Na) to 1687 cm^{-1} for heavy-metal (Ni or Cu) complexes. At nearly 100% humidity, the cations did not distinctly affect band positions of the adsorbed aflatoxin molecules. We concluded that, under dry conditions, major bonding between adsorbed aflatoxin B_1 and smectite was ion-dipole interactions and coordination between exchangeable cations and carbonyl groups. Under humid conditions, H-bonding between carbonyl groups and exchangeable-cation hydration-shell water was the dominant bonding force.

1. Introduction

Using clay minerals, mainly montmorillonite, to alleviate aflatoxin toxicity was started in the late 1970s (Masimango et al., 1978, 1979). Bentonites, the montmorillonite-rich clays, are broadly distributed around the world. Several bentonites from USA, Japan, Mexico, India, China, and Argentina were shown effective in binding aflatoxins and in reducing or diminishing aflatoxin bioavailability (Chaturvedi et al., 2002; Desheng et al., 2005; Magnoli et al., 2008; Márquez and Hernandez, 1995; Nahm, 1995; Phillips et al., 1988). Bentonites were tested in numerous animal feed trials which included chickens, turkey poults, ducklings, pigs, lambs, mink, trout, tilapia fish, dairy cows, and goats (e.g., Abdel-Wahhab et al., 2005; Bailey et al., 2006; Bonna et al., 1991; Cerdchai et al., 1990; Colvin et al., 1989; Harvey et al., 1991a,b; Kubena et al., 1991; Smith et al., 1994; Winfree and Allred, 1992). Recent clinical trials of a bentonite NovaSil added to human diets showed promising results in reducing concentrations of aflatoxin B_1–albumin adduct in blood samples and of aflatoxin M_1, a metabolite of aflatoxin B_1, in urine samples (Afriyie-Gyawu et al., 2008a,b; Phillips et al., 2008; Wang et al., 2008).

Stimulated by the effectiveness of certain bentonites in reducing aflatoxin toxicity, several articles discussed critical mineralogical and chemical properties of bentonites related to aflatoxin adsorption (Dixon et al., 2008; Kannewischer et al., 2006; Mulder et al., 2008; Tenorio et al., 2008). Efforts were made to modify smectites or zeolites with inorganic cations, organic quaternary ammonium, and phosphatidylcholine to enhance the minerals' adsorption capacity for aflatoxin (Dakovic et al., 2005, 2008; Wicklein et al., 2009). Interference of other food ingredients in corn meal on the adsorption of aflatoxin was investigated by Jaynes et al. (2007). To select or modify smectites that effectively detoxify aflatoxins and to enhance smectite selectivity in the presence of feed or food ingredients, a molecular-level understanding of aflatoxin–smectite reaction mechanisms is critically needed.

1.1. Adsorption site of aflatoxin on smectite

As smectites are expandable 2:1 phyllosilicate minerals, the external basal surfaces, edges, and the interlayer space are possible adsorption sites for aflatoxins. Some authors concluded that the adsorption occurred only on the external or the edge surfaces (Desheng et al., 2005), others suggested that the interlayer space was accessible to the toxins as well (Kannewischer et al., 2006 Phillips et al., 2002;). Based on computational simulation and an observation of aflatoxin adsorption reduction after collapsing the Ca-bentonite NovaSil by heating, Phillips et al. (1995) proposed that aflatoxin could be bound at edges, within the interlayer, and at the basal surfaces of smectite by selective chemisorption. Kannewischer et al. (2006) showed that interlayer adsorption could occur when an aflatoxin–benzene–acetonitrile solution was evaporated with bentonites. As water is the most common solvent, the occurrence of interlayer adsorption in the presence of water needs to be tested.

* Corresponding author. Tel.: +1 979 8628476; fax: +1 979 8450456.
E-mail addresses: yjd@tamu.edu (Y. Deng), anabarrientos@neo.tamu.edu (A.L.B. Velázquez), fbilles@mail.bme.hu (F. Billes), j-dixon@tamu.edu (J.B. Dixon).

0169-1317/$ – see front matter © 2010 Elsevier B.V. All rights reserved.
doi:10.1016/j.clay.2010.07.008

1.2. Debate on aflatoxin/smectite bonding mechanisms

The leading hypothesis on the bonding mechanism between adsorbed aflatoxins and smectites was the electron donor–acceptor (EDA) model. Other models such as selective chemisorption, H-bonding, and bonding through furan rings were proposed. It was not clear which mechanism was dominant in aflatoxin adsorption.

1.2.1. Electron donor–acceptor (EDA) model

This model was proposed by Haderlein et al. (1996) for the specific adsorption of nitroaromatic compounds by smectite. It was adapted to explain aflatoxin adsorption to smectite: each aflatoxin molecule had two carbonyl groups containing two carbons with a partial positive charge that could share electrons from the negatively-charged smectite surface (Phillips, 1999; Phillips et al., 2006, 2008).

1.2.2. Selective chemisorption

Phillips et al. (1995) reported that the adsorption enthalpy of aflatoxin on smectite was about −40 kJ mol^{-1}, and that the carbonyl-stretching bands of aflatoxin between 1700 and 1750 cm^{-1} disappeared upon reaction with the Ca-bentonite NovaSil and two new bands between 1400 and 1600 cm^{-1} appeared. They proposed that the two carbonyl groups should readily form chelates with transition metals possessing unfilled *d* orbitals, and that aflatoxin formed a mononuclear bidentate chelate with transition metals in NovaSil.

1.2.3. Hydrogen bonding and bonding through furan ring

Desheng et al. (2005) proposed that formation of a double hydrogen-bond between aflatoxin and montmorillonite edge sites was the main chemisorption reaction mechanism. Tenorio et al. (2008) proposed that binding was due to the coordination between exchange cations and two oxygens of the coumarin moiety (Ring D, Fig. 1). They further suggested that epoxidation of the furan (Ring A in Fig. 1) might occur on the adsorbed aflatoxins and that the epoxidized furan ring contributed to the bonding of the toxin to smectites.

1.2.4. Other possible bonding models based on similar oxygen-containing organics

Carbonyl groups in esters, amides, ketones, and aldehydes were adsorbed by expandable clay minerals mainly via ion-dipole interactions and coordination between the exchange cations and the carbonyl groups (Deng and Dixon, 2002; Theng, 1974). H-bonding between the carbonyl groups and water in the hydration shells were proposed for many of the carbonyl functional groups. As an aflatoxin molecule contains six oxygens, including the two carbonyl groups (Fig. 1), similar ion-dipole and H-bonding interactions should occur.

It is evident that there are several important unsettled questions regarding the adsorption site and bonding mechanisms. Both experimental and computational data are needed to clarify these questions. The objectives of this study were to test aflatoxin molecule access to smectite interlayers for adsorption in the presence of water and to elucidate bonding mechanisms of adsorbed aflatoxin B_1 molecules to smectite.

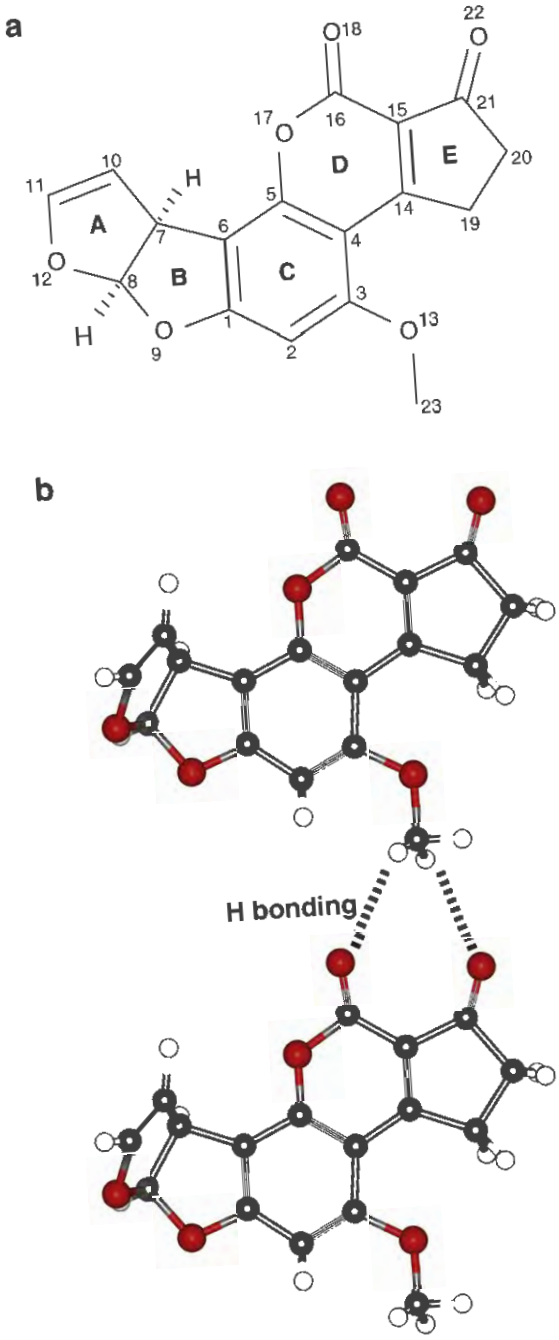

Fig. 1. a: Schematic representation of aflatoxin B_1 molecule, ring labels and numbered atom positions are after Billes et al. (2006). b: Aflatoxin B_1 molecules form strings of coplanar layers in one of three crystal forms, in each string, H-bonding between the methoxy group and two carbonyl oxygens links the molecules together(van Soest and Peerdeman, 1970a,b).

2. Materials and methods

2.1. Preparation of Ca–smectite and aflatoxin B_1 adsorption isotherm

The <2 μm clay fraction of a Ca-bentonite from Southern Clay Products, Inc. (Gonzales, TX) was used in our early study (Deng et al., 2003). We followed the same procedure to collect the clay fraction from the same bentonite batch. The collected clay fraction was saturated with Ca^{+} and then freeze dried (VirTis 25 Liter FreezeMobile, the VirTis Company, Gardiner, New York). The clay fraction had a cation exchange capacity of 81 cmol(c)kg^{-1} and a specific surface area of 790 m^2 g^{-1}. Smectite was the major mineral in the clay fraction. A small amount of opal-CT was detected by X-ray diffraction and infrared spectroscopy analyses. The adsorption capacity of the smectite for aflatoxin B_1 was determined with batch experiment described by Kannewischer et al. (2006).

2.2. Synthesis of aflatoxin–smectite complexes

Aflatoxin B_1/acetonitrile stock solution (1000 μg mL^{-1}) was prepared by dissolving 50 mg aflatoxin from *Aspergillus flavus* (Sigma-Aldrich Inc. St. Louis, MO) in 50 mL acetonitrile in a volumetric flask wrapped with aluminum foil and was stored at 4 °C (Kannewischer et al., 2006). A supersaturated aqueous aflatoxin B_1 solution, which

had an equivalent concentration of 100 μg mL^{-1} aflatoxin B_1, was prepared by diluting the 1000 μg mL^{-1} aflatoxin/acetonitrile stock solution with deionized water. Fifty milliliters of the supersaturated aqueous aflatoxin B_1 solution was added to 100 mL smectite dispersion containing 50 mg Ca-smectite in a 250-mL centrifuge bottle. The bottle was shaken overnight at 200 rpm on an orbital shaker (Cole-Parmer, model 51501-20, Vernon Hills, Illinois). After centrifugation and decanting the supernatant, the settled smectite was redispersed in 100 mL water, and mixed with another 50 mL supersaturated aqueous aflatoxin B_1 solution for an additional exposure to aflatoxin. After centrifugation, the aflatoxin–smectite complex was transferred to a 15-mL centrifuge tube and washed twice with deionized water (15 mL each time). The resulting complex was dispersed in 2.0 mL water.

2.2.1. Aflatoxin B_1–smectite complexes saturated with Na, K, Ca, Mg, Al, La, Mn, Ni, or Cu

To investigate the possible influence of exchange cation on bonding strength, cations in the aflatoxin B_1–smectite complex were replaced with Na^+, K^+, Ca^{2+}, Mg^{2+}, Al^{3+}, La^{3+}, Mn^{2+}, Ni^{2+}, and Cu^{2+}. The Ca^{2+} was included here to account for washing effect. Solutions of 0.5 M NaCl, 0.5 M KCl, 0.25 M C_aCl_2, and 0.25 M $MgCl_2$ were prepared in deionized water. The pHs of the solutions were in the range of 5 to 5.5. Solutions of 0.17 M $Al(NO_3)_3$, 0.05 M $LaCl_3$, 0.1 M $MnCl_2$, 0.1 M $Ni(NO_3)_2$, 0.1 M C_uCl_2 were prepared in 1 mM HCl solution. These HCl-prepared solutions had pHs between 2.8 and 3.0. An aliquot of the aflatoxin B_1–smectite complex dispersion containing 5 mg complex was treated two times with 10 mL of each electrolyte solution in separate centrifuge tubes. The tubes were shaken for 4 h and centrifuged. After cation exchange, each of the resulting complexes was washed two times with 10-mL water to remove excess electrolytes.

2.3. Variable temperature X-ray diffraction (XRD) analysis

Smectite or aflatoxin B_1–smectite complex dispersion was air dried on a zero-background quartz slide (19.6 × 14.8 × 1.4 mm). The XRD patterns at elevated temperatures up to 500 °C were recorded in a reactor chamber XRK 900 (Anton Paar Gmbh, Graz, Austria) on a D8 Bruker Advance X-ray diffractometer. A heating rate of 0.1 °C/s was used during the analysis. The temperature was maintained constant as each XRD pattern was recorded.

2.4. Infrared spectroscopy analysis

The infrared spectrum of aflatoxin B_1 was recorded with KBr pellet (about 0.5 mg aflatoxin in 300 mg KBr). To record the infrared spectrum of an aflatoxin–smectite complex, the complex dispersion was dried on a polished 25 × 2 mm ZnS disc (ClearTran, International Crystal Labs, Garfield, New Jersey). For nearly 100% humidity, a piece of wet Kimwipe tissue was kept between the sample disc and a blank disc sealed with a rubber ring. Spectra were also recorded without the wet Kimwipe tissue (between room humidity and 100% humidity), at room humidity (40%–68%), and at nearly 0% humidity (dry N_2 purge). Spectra were recorded in transmission mode with a resolution of 1 cm^{-1} on FTIR System 2000 and Spectrum 100 infrared spectrometers (Perkin-Elmer). Thirty two or 64 scans were collected and averaged for each spectrum.

2.5. Scaling of theoretical IR bands of aflatoxin

Billes et al. (2006) reported the theoretical infrared spectrum of aflatoxin B_1 based on quantum chemical calculation. Individual scale factors for internal coordinates of the molecule were refined so the theoretical positions matched the experimental values measured in this study. A custom algorithm was used to refine the scale factors by searching local minima step-by-step for every internal coordinate group. The mean deviation of the measured and the computed band positions was 8 cm^{-1} for all bands in the range 400–4000 cm^{-1}.

3. Results and discussion

3.1. Indirect evidence of aflatoxin B_1 intercalation of smectite from adsorption isotherms

The adsorption of aflatoxin B_1 on this smectite sample showed an L-type isotherm curve (Fig. 2). The L-shape, not an S-shaped isotherm curve, suggests that a multiple layer adsorption on external surface was unlikely. A maximum adsorption capacity of 0.45 mol kg^{-1} (or 14% by mass) was calculated from the Langmuir equation fit parameters. Our calculation based on the geometric sizes of the nearly-planar aflatoxin B_1 molecule reported by Phillips et al. (1995) suggests that one adsorbed aflatoxin B_1 molecule occupied about 1.38 nm^2 surface area. The 0.45 mol kg^{-1} adsorption capacity required a specific surface area of 370 m^2 g^{-1}. Such a high surface area demand implies that the molecules intercalated smectite interlayer. If aflatoxin molecules intercalated smectite, the sandwiched molecules would require twice the molecular area; i.e. aflatoxin molecules would occupy both interlayer surfaces of smectite for a specific surface area of 740 m^2 g^{-1}. This was close to the sample's specific surface area of 790 m^2 g^{-1} and implied that aflatoxin molecules occupied nearly all of the surface area.

3.2. Aflatoxin intercalation of smectite as revealed by XRD analysis

The aflatoxin–smectite complex preserved a basal spacing greater than 1.20 nm up to 400 °C (Fig. 3) whereas the smectite collapsed to less than 1.0 nm at 150 °C and higher temperatures. The different responses to heating suggest that an organic residue remained in the aflatoxin–smectite complex interlayer after heating. In other words, aflatoxin B_1 intercalated the smectite when water was used as the solvent during the synthesis.

3.3. Infrared evidence on bonding between aflatoxin and smectite

Infrared bands in the range of 1300–1800 cm^{-1} offered the most useful information about bonding between aflatoxin B_1 and smectite. Several infrared bands of adsorbed aflatoxin shifted compared with those of the pure aflatoxin B_1. These shifts were affected by humidity and exchange cation.

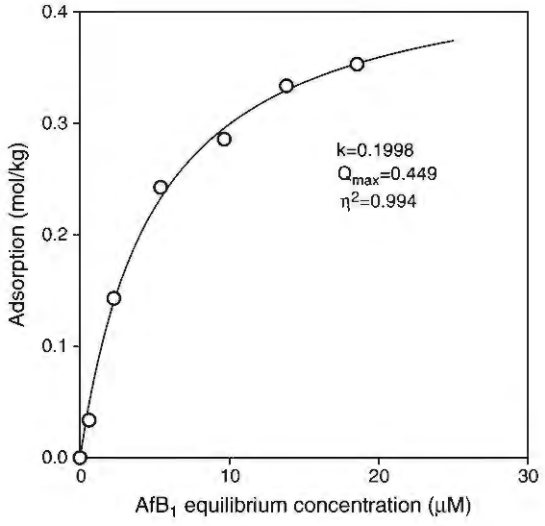

Fig. 2. Adsorption isotherm of aflatoxin B_1 on Ca–smectite from water.

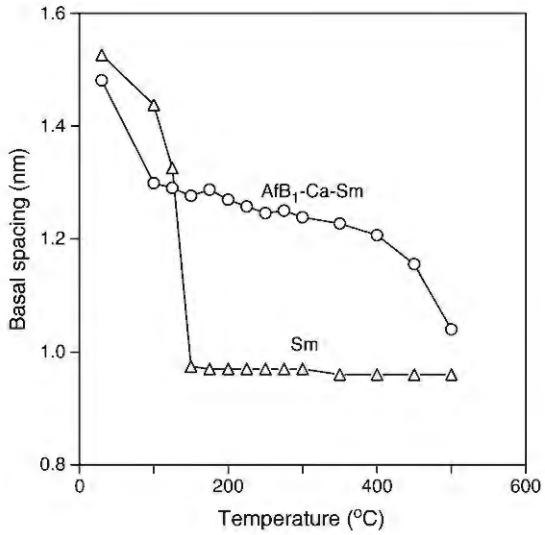

Fig. 3. The basal spacings of smectite (Sm) and aflatoxin B_1–Ca–smectite (AfB_1–Ca–Sm) complex after heating at elevated temperatures.

3.3.1. Humidity-reversible infrared band shifts of adsorbed aflatoxin

Several infrared bands of the adsorbed aflatoxin shifted when the humidity was changed. The in-phase carbonyl (C O) vibration of Cu-saturated aflatoxin B_1–smectite complex (AfB_1–Cu–Sm) occurred at 1744 cm^{-1} at nearly 100% humidity (Fig. 4, spectrum *a*). The 1744 cm^{-1} band shifted to 1687 cm^{-1} (57 cm^{-1} red shift) when the complex was exposed to 68% relative humidity. Further moisture removal resulted in only little changes in band position. During the drying process, other band shifted as well: 1595 cm^{-1} to 1581 cm^{-1}, 1550 cm^{-1} to 1537 cm^{-1}, 1496 to 1506 cm^{-1} (Fig. 4, spectra *a*,*b*,*c*1 and *d*). The shifts of aflatoxin infrared bands with humidity were reversible. For example, when the air dried or N_2 dried complex was re-exposed to 100% humidity, all of the aflatoxin bands (Fig. 4, spectrum *c2*) shifted back to the same positions as the starting 100% humidity pattern (Fig. 4, spectrum *a*).

3.3.2. Humidity-reversible color changes of aflatoxin/smectite complexes

Exchangeable cations and humidity affected the color of aflatoxin/smectite complexes. The Na-, K-, Ca-, and Mg-saturated complexes were white, whereas, the Cu-, Mn-, Ni-, Al-, and La-saturated complexes were yellow when dried. Changes in humidity produced reversible color changes. For example, the air dried AfB_1–Cu–Sm complex was pale yellow, it changed to dark yellow when it was dried at nearly 0% humidity in N_2. The dark yellow color faded when the sample was exposed to 100% humidity, but the yellow color recovered when the sample was re-exposed to lower humidities.

The reversible infrared band shifts and color changes of the complexes suggest that the interlayer space of the aflatoxin–smectite complexes were still accessible to water molecules. The major driving force for interlayer water entry was the hydration energy of exchangeable cations. Hence, aflatoxin molecules must be distributed and oriented for interlayer water pathways to be continuous. It also implies that interlayer aflatoxin molecules were isolated from each other.

3.3.3. IR band positions of adsorbed aflatoxin at 100% humidity

The infrared spectra of aflatoxin in the aflatoxin–smectite complexes were essentially the same at 100% humidity for the nine exchange cations (K, Na, Ca, Mg, Al, La, Mn, Ni, and Cu), (Fig. 5), which suggests a similar bonding mechanism between adsorbed aflatoxin and smectite at high humidity.

3.3.4. Adsorbed aflatoxin IR band shift as a function of exchange cation at near 0% humidity

Several adsorbed aflatoxin-molecule IR bands shifted as the exchange cations were replaced (Table 1 and Fig. 6). The largest red-shift was for the in-phase stretching vibration of the two-carbonyl bonds. A highest frequency of 1736 cm^{-1} was for the K-saturated complex and the lowest frequency of 1687 cm^{-1} (~50 cm^{-1} lower) was for Al- or Cu-saturated complexes. The amount of red shift with cations was apparently related to cation size and charge, and d-orbital occupancy completeness. Cations of higher valence, smaller size, and unpaired d-orbitals induced greater IR band red shifts.

We assigned free-aflatoxin 1692 and 1684 cm^{-1} bands (Fig. 6, a) to opposite-phase stretching vibrations of the two carbonyl C O bonds. The bands merged as broad shoulder bands at 1658 cm^{-1} next to the dominant band at 1635 cm^{-1} in all complexes at 100% humidity (Fig. 5). At nearly 0% humidity, only the K-saturated aflatoxin–smectite complex showed a distinct shoulder band at similar location 1657 cm^{-1}. The bands in other complexes merged to the strong water bending band centered at 1630 cm^{-1}. We interpreted these observations as the result of red shifts of the opposite-phase stretching vibrations of the carbonyl groups in the complexes.

Red shifts were observed on bands related to the C C bonds (C14C15 in Fig. 1) at 1594 and 1550 cm^{-1} when the cations were transitional metal cations or trivalent cations at 0% humidity (Fig. 6).

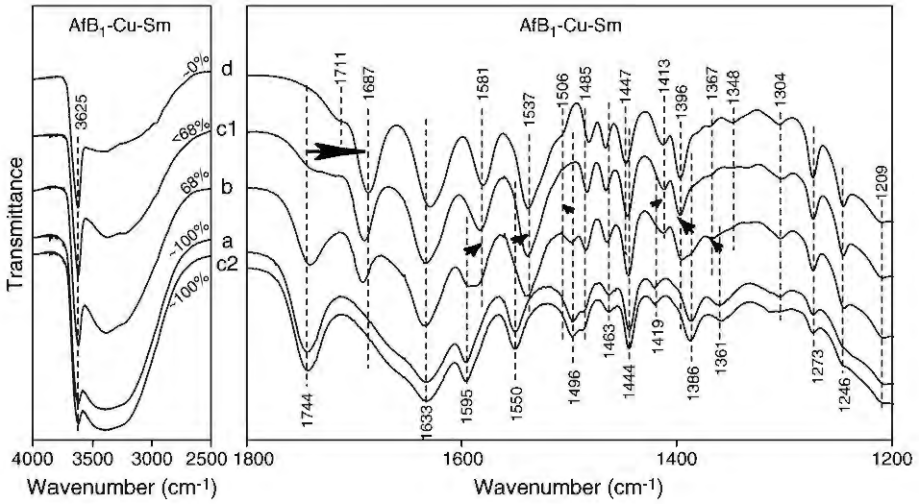

Fig. 4. Infrared spectra of aflatoxin B_1–Cu–smectite complex recorded at different humidities showing reversible band shifts with humidity: humidity was reduced from near 100% (spectrum a), 68% (spectrum b), to <68% by partial N_2 purge (spectrum c1), returned to 100% (c2), and then near 0% by full N_2 purge (spectrum d).

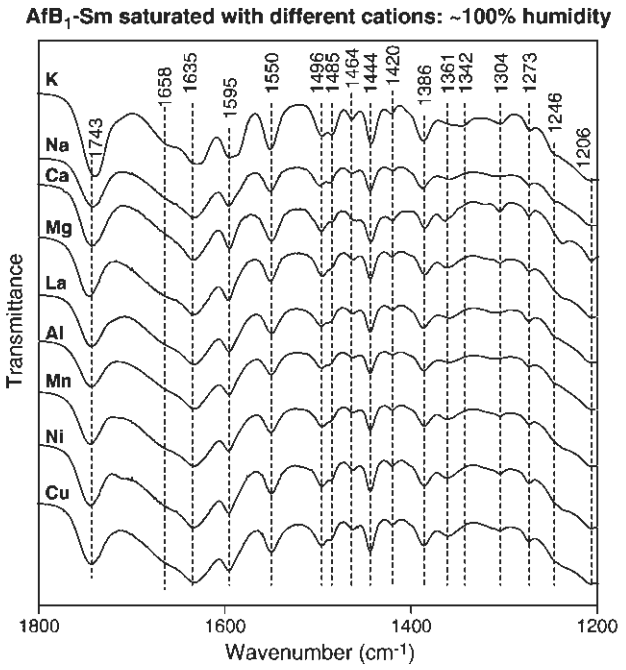

Fig. 5. Infrared spectra of aflatoxin B_1–smectite complexes saturated with different cations at nearly 100% humidity.

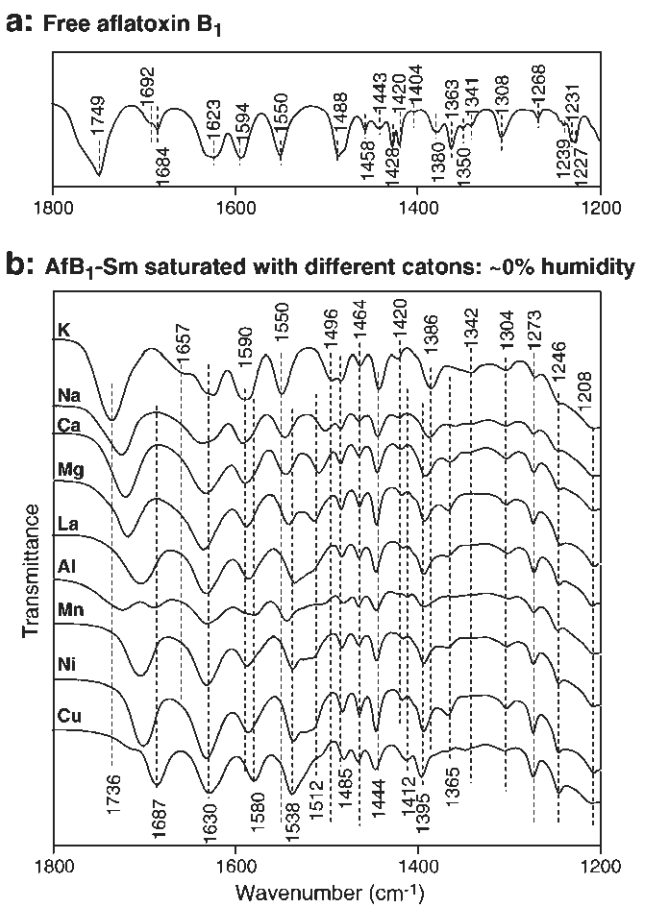

Fig. 6. Infrared spectra of free aflatoxin B_1 (a) and of aflatoxin B_1–smectite complexes saturated with different cations at nearly 0% humidity (b).

The 1594 cm^{-1} band mainly originated from the benzene ring and the C C double bonds (C14C15 and C10C11 in Fig. 1) whereas the 1550 cm^{-1} mainly from the stretching vibration of the C C double bond (C14C15 in Fig. 1). The red shifts suggest that the C C bond was weakened by the bonding between the aflatoxin and the exchange cations.

The fused 1488 cm^{-1} bands of pure aflatoxin B_1 (Fig. 6, a) arose from deformation bands of the rings (e.g., D and E in Fig. 1) and the deformation vibrations of the C–H groups. This band occurred at 1485 cm^{-1} in the complexes and did not shift with humidity or cations. The 1496 cm^{-1} band shifted to higher frequencies in the presence of transition metal or trivalent cations. The blue shifts were more likely related to the ring deformation in rings D and E.

3.3.5. Minor infrared band shifts on benzene ring and C–H groups

The doublet bands at about 1623 cm^{-1} in free aflatoxin (Fig. 6, a) were mainly due to the stretching vibrations of the benzene ring (Table 1). The 1464 and 1444 cm^{-1} bands in the complexes were mainly due to the in-plane and out-of-plane bending vibrations of the C–H groups. These bands did not shift with cations or humidity, which suggests that the

Table 1
Infrared band position and assignments for free aflatoxin B_1 and aflatoxin B_1 in AfB_1–smectite complexes for different exchange cations at ~0% humidity.

Free AfB_1		AfB_1–smectite saturated with									Major vibrations[a]
Measured	Computed	K^+	Na^+	Ca^{2+}	Mg^{2+}	Al^{3+}	La^{3+}	Mn^{2+}	Ni^{2+}	Cu^{2+}	
1749	1805	1736	1725	1727	1717	1703	1689	1705	1701	1687	In-phase νC = O
1684	1734	1654									Opp.-phase νC = O
1623	1609	1624	1636	1635	1636	1632	1631	1632	1632	1630	βCO, νCCd, βH_2O
1594	1589	1588	1592	1592	1588	1585	1579	1587	1586	1580	νCCc, νC = C
1550	1553	1550	1545	1546	1542	1535	1544	1537	1536	1538	νC = C, νCCc
1488	1474	1496	1502	1506	1513		1522	1522			νCCc
		1484	1484	1484	1484	1483	1482	1483	1482	1479	νCCc
1458	1459	1463	1465	1463	1464	1464	1465	1465	1464	1466	γCHo
1443	1445	1442	1444	1444	1445	1446	1446	1445	1446	1446	γCHo
1427	1426										βCHm, γCHo
1419	1419	1422	1419	1420	1417	1416	1411	1416	1417	1412	γCHo
1378	1398	1386	1387	1387	1392	1393	1393	1393	1394	1395	γCHo
1363	1365	1354	1359	1364	1367	1368		1367	1367	1369	νC-O, νCCc
1350	1351										νCCc, νC-O
1341	1340	1342	1342								γCHo, βCHa
1308	1322	1303	1303	1303	1303	1301	1300	1302	1302	1307	νCCc, νCCo,
1268	1274	1271	1273	1274	1273	1272	1273	1273	1273	1273	νCCo, βCHo
1240	1245	1244	1246	1236	1243	1245	1246	1245	1245	1245	βCHo, βCHa
1231	1226										βCHo, γCHo
1227	1223										βCHo
1200	1205	1207	1207	1205	1206	1208	1207	1207	1207	1207	βCHo, γCHo

[a] ν: stretching, β: in-plane deformation, γ: out-of-plane deformation; a: ring A, m: methyl, o: diverse.

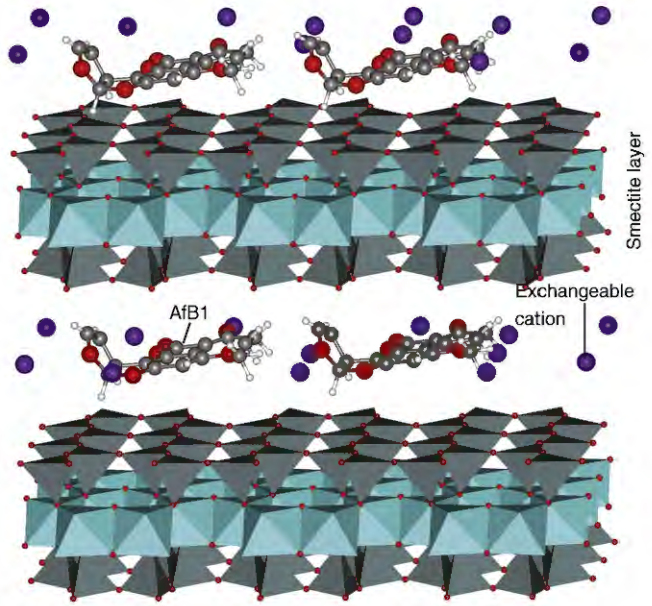

Fig. 7. Proposed model of an aflatoxin intercalated smectite. Interlayer water molecules were not shown.

benzene ring or the C–H bonds were not involved in the bonding of aflatoxin molecules to smectite. Small band shifts or intensity changes were observed on bands between 1428 and 1208 cm^{-1} when humidity or cations were changed (Figs. 5 and 6). The precise meanings of the small shifts or intensity changes of these bands deserve more theoretical analysis.

3.4. Proposed aflatoxin–smectite bonding model

We proposed that aflatoxin molecules occupied the interlayer space together with exchange cations and water molecules (Fig. 7.). Aflatoxin molecules were bonded to smectite by H-bonding between the carbonyl oxygens and hydration-shell water at high humidity, whereas, bonding was by direct ion-dipole interactions or exchange cation/carbonyl oxygen coordination under dry conditions (Fig. 8). For the high-humidity, H-bonding mode via water bridges, the cations did not affect aflatoxin/smectite bond strength. In the ion-dipole interaction/coordination mode, the cations with higher valence, smaller size, or with unpaired electrons in d-orbits interacted more strongly with the aflatoxin molecules. The intensities of aflatoxin infrared bands in the aflatoxin–smectite complexes after extensive washing with electrolytes and water (Figs. 4–6) were nearly the same as the complex before washing, which suggests high stability of interlayer-adsorbed aflatoxin. The low water solubility (about 30 ppm) of aflatoxin B_1 in water implied it prefers a hydrophobic surface. We speculated that the stability and selectivity of aflatoxin adsorption would be enhanced when the size and the polarity of aflatoxin molecule match those of the interlayer nanoscale domains between the exchange cations in smectite.

3.4.1. Simultaneous occurrence of two types of bonding

When the humidity was slightly lower than 100%, there were two infrared bands occurred at 1744 and 1687 cm^{-1} on the spectrum *b* of the aflatoxin B_1–Cu–smectite complex (Fig. 4, spectrum b). Both bands originated from the in-phase stretching vibrations of the two carbonyl bonds. The occurrence of these two bands suggests two types of bonding (H-bonding and coordination) occurred simultaneously between aflatoxin and smectite. At 68% and nearly 0% humidities, there was a shoulder infrared band at 1711 cm^{-1} on the spectra *c1* and *d* in Fig. 4, which was 33 cm^{-1} lower than the 1744 cm^{-1} band at 100% humidity. The shoulder band at 1711 cm^{-1} on spectra *c1* and *d* was attributed to the H-bonded aflatoxin. The lower frequency of the band suggests that the H-bonding under drier condition was stronger than that at 100% humidity.

4. Conclusions

The high aflatoxin adsorption capacity of smectite and the persistence of the aflatoxin–smectite complex prepared in water after heating indicate that aflatoxin molecules could intercalate smectite in water. The fact that different humidities and exchange cations shifted adsorbed aflatoxin infrared bands suggests that aflatoxin molecules were adsorbed to smectite through direct ion-dipole interactions and coordination between exchange cations and the carbonyl oxygens at low humidity. At high humidity, H-bonding was between cation hydration-shell water and the carbonyls. These bonding modes were consistent with the interactions of common carbonyl compounds with smectite.

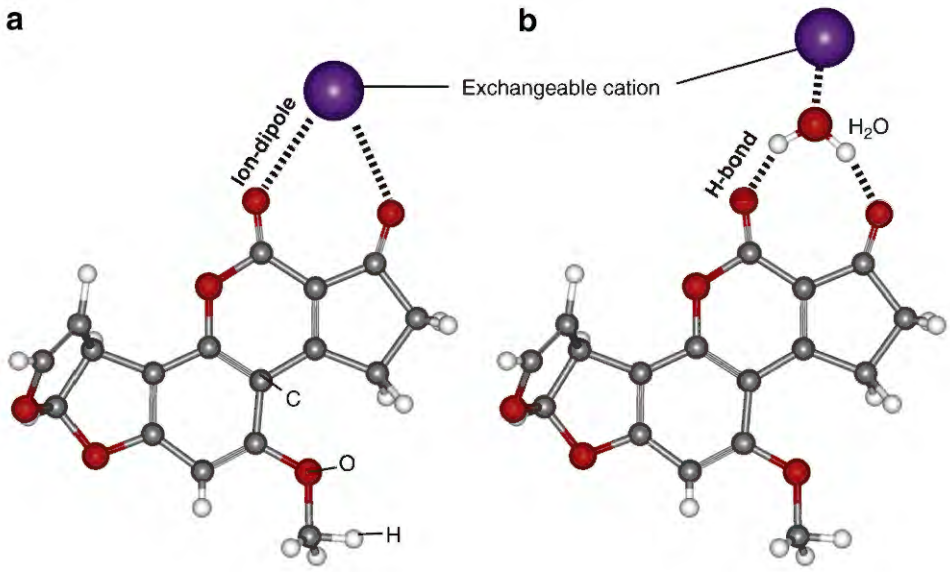

Fig. 8. Proposed bonding mechanisms: (a) ion-dipole interaction/coordination between the two carbonyl oxygens with exchange cation, and (b) H-bonding between carbonyl functional groups and exchange-cation hydration-shell water.

Acknowledgements

Funding was supplied by the Texas AgrilLife Research and Texas Corn Producers Board. The Laboratory for Molecular Simulation at Texas A&M University provided the Materials Studio software to generate the models.

References

Abdel-Wahhab, M.A., Hasan, A.M., Aly, S.E., Mahrous, K.F., 2005. Adsorption of sterigmatocystin by montmorillonite and inhibition of its genotoxicity in the Nile tilapia fish (*Oreachromis nilaticus*). Mutat. Res.-Gen. Tox. En. 582 (1–2), 20–27.

Afriyie-Gyawu, E., Ankrah, N.A., Huebner, H.J., Ofosuhene, M., Kumi, J., Johnson, N.M., Tang, L., Xu, L., Jolly, P.E., Ellis, W.O., Ofori-Adjei, D., Williams, J.H., Wang, J.S., Phillips, T.D., 2008a. NovaSil clay intervention in Ghanaians at high risk for aflatoxicosis. I. Study design and clinical outcomes. Food Addit. Contam. A-Chem. 25 (1), 76–87.

Afriyie-Gyawu, E., Wang, Z., Ankrah, N.A., Xu, L., Johnson, N.M., Tang, L., Guan, H., Huebner, H.J., Jolly, P.E., Ellis, W.O., Taylor, R., Brattin, B., Ofori-Adjei, D., Williams, J. H., Wang, J.S., Phillips, T.D., 2008b. NovaSil clay does not affect the concentrations of vitamins A and E and nutrient minerals in serum samples from Ghanaians at high risk for aflatoxicosis. Food Addit. Contam. A-Chem. 25 (7), 872–884.

Bailey, C.A., Latimer, G.W., Barr, A.C., Wigle, W.L., Haq, A.U., Balthrop, J.E., Kubena, L.F., 2006. Efficacy of montmorillonite clay (NovaSil PLUS) for protecting full-term broilers from aflatoxicosis. J. Appl. Poultry Res. 15 (2), 198–206.

Billes, F., Móricz, A.M., Tyihák, E., Mikosch, H., 2006. Simulated vibrational spectra of aflatoxins and their demethylated products and the estimation of the energies of the demethylation reactions. Spectrochim. Acta A 64 (3), 600–622.

Bonna, R.J., Aulerich, R.J., Bursian, S.J., Poppenga, R.H., Braselton, W., Watson, G.L., 1991. Efficacy of hydrated sodium calcium aluminosilicates and activated charcoal in reducing the toxicity of dietary aflatoxin to mink. Arch. Environ. Contam. Toxicol. 20 (3), 441–447.

Cerdchai, R., Paisansarakit, A., Khajarern, J., 1990. Effect of hydrated sodium calcium aluminosilicate (NovaSil) on reducing aflatoxicosis in ducks. Proceedings of the 7th FAVA Congress: Pattay, p. 391.

Chaturvedi, V.B., Singh, K.S., Agnihotri, A.K., 2002. In vitro aflatoxin adsorption capacity of some indigenous aflatoxin adsorbents. Indian J. Anim. Sci. 72 (3), 257–260.

Colvin, B.M., Sangster, L.T., Haydon, K.D., Beaver, R.W., Wilson, D.M., 1989. Effect of a high affinity aluminosilicate sorbent on prevention of aflatoxicosis in growing pigs. Vet. Hum. Toxicol. 31 (1), 46–48.

Dakovic, A., Tomasevic-Canovic, M., Dondur, V., Rottinghaus, G.E., Medakovic, V., Zaric, S., 2005. Adsorption of mycotoxins by organozeolites. Colloids Surf. B 46 (1), 20–25.

Dakovic, A., Matijasevic, S., Rottinghaus, G.E., Ledoux, D.R., Butkeraitis, P., Sekulic, Z., 2008. Aflatoxin B_1 adsorption by natural and copper modified montmorillonite. Colloids Surf. B 66 (1), 20–25.

Deng, Y., Dixon, J.B., 2002. Soil organic matter and organic-mineral interactions. In: Dixon, J.B., Schulze, D.G. (Eds.), Soil Mineralogy with Environmental Applications. of SSSA Book Series, 7. Soil Science Society of America, Inc., Madison, Wisconsin, USA, pp. 69–107.

Deng, Y., Dixon, J.B., White, G.N., 2003. Intercalation and surface modification of smectite by two non-ionic surfactants. Clays Clay Miner. 51 (2), 150–161.

Desheng, Q., Fan, L., Yanhu, Y., Niya, Z., 2005. Adsorption of aflatoxin B-1 on montmorillonite. Poult. Sci. 84 (6), 959–961.

Dixon, J.B., Kannewischer, I., Tenorio Arvide, M.G., Barrientos Velazquez, A.L., 2008. Aflatoxin sequestration in animal feeds by quality-labeled smectite clays: an introductory plan. Appl. Clay Sci. 40, 201–208.

Haderlein, S.B., Weissmahr, K.W., Schwarzenbach, R.P., 1996. Specific adsorption of nitroaromatic explosives and pesticides to clay minerals. Environ. Sci. Technol. 30 (2), 612–622.

Harvey, R.B., Kubena, L.F., Phillips, T.D., Corrier, D.E., Elissalde, M.H., Huff, W.E., 1991a. Diminution of aflatoxin toxicity to growing lambs by dietary supplementation with hydrated sodium calcium aluminosilicate. Am. J. Vet. Res. 52 (1), 152–156.

Harvey, R.B., Phillips, T.D., Ellis, J.A., Kubena, L.F., Huff, W.E., Petersen, H.D., 1991b. Effect on aflatoxin M1 residues in milk by addition of hydrated sodium calcium aluminosilicate to aflatoxin-contaminated diets of dairy cows. Am. J. Vet. Res. 52 (9), 1556–1559.

Jaynes, W.F., Zartman, R.E., Hudnall, W.H., 2007. Aflatoxin B-1 adsorption by clays from water and corn meal. Appl. Clay Sci. 36 (1–3), 197–205.

Kannewischer, I., Tenorio, A.M.G., White, G.N., Dixon, J.B., 2006. Smectite clays as adsorbents of aflatoxin B1: initial steps. Clay Sci. 12 (Supplement 2), 199–204.

Kubena, L.F., Huff, W.E., Harvey, R.B., Yersin, A.G., Elissalde, M.H., Witzel, D.A., Giroir, L.E., Phillips, T.D., Petersen, H.D., 1991. Effects of a hydrated sodium calcium aluminosilicate on growing turkey poults during aflatoxicosis. Poult. Sci. 70 (8), 1823–1830.

Magnoli, A.P., Cabaglieri, L.R., Magnoli, C.E., Monge, J.C., Miazzo, R.D., Peralta, M.F., Salvano, M.A., Rosa, C.A.R., Dalcero, A.M., Chiacchiera, S.M., 2008. Bentonite performance on broiler chickens fed with diets containing natural levels of aflatoxin B_1. Rev. Bras. Med. Vet 30 (1), 55–60.

Márquez, R.N., Hernandez, I.T.D., 1995. Aflatoxin adsorbent capacity of two Mexican aluminosilicates in experimentally contaminated chick diets. Food Addit. Contam. 1995, 431–433.

Masimango, N., Remacle, J., Ramaut, J.L., 1978. The role of adsorption in the elimination of aflatoxin B1 from contaminated media. Eur. J. Appl. Microbiol. Biotechnol. 6 (1), 101–105.

Masimango, N., Remacle, J., Ramaut, J., 1979. Elimination of aflatoxin B1 from contaminated media by swollen clays. Ann. Nutr. Aliment. 33 (1), 137–147.

Mulder, I., Tenorio Arvide, M.G., White, G.N., Dixon, J.B., 2008. Smectite clay sequestration of aflatoxin B1: mineral dispersivity and morphology. Clays Clay Miner. 56, 559–571.

Nahm, K.H., 1995. Prevention of aflatoxicosis by addition of antioxidants and hydrated sodium calcium aluminosilicate to the diet of young chicks. Nippon Kakin Gakkaishi 32 (2), 117–127.

Phillips, T.D., 1999. Dietary clay in the chemoprevention of aflatoxin-induced disease. Toxicol. Sci. 52 (2), 118–126.

Phillips, T.D., Kubena, L.F., Harvey, R.B., Taylor, D.R., Heidelbaugh, N.D., 1988. Hydrated sodium calcium aluminosilicate: a high affinity sorbent for aflatoxin. Poult. Sci. 67, 243–247.

Phillips, T.D., Sarr, A.B., Grant, P.G., 1995. Selective chemisorption and detoxification of aflatoxins by phyllosilicate clay. Nat. Toxins 3 (4), 204–213.

Phillips, T.D., Lemke, S.L., Grant, P.G., 2002. Characterization of clay-based enterosorbents for the prevention of aflatoxicosis. Mycotoxins and Food Safety. Vol. 504 of Advances in Experimental Medicine and Biology. Kluwer Academic/Plenum Publ, pp. 157–171.

Phillips, T.D., Afriyie-Gyawu, E., Wang, J.S., Williams, J.O., Huebner, H., 2006. The potential of aflatoxin sequestering clay. In: Barug, D., Bhatnagar, D., van Egmond, H.P., van Der Kamp, J.W., van Osenbruggen, W.A., Visconti, A. (Eds.), The Mycotoxin Factbook: Food and Feed Topics. Wageningen Academic Publishers, Wageningen, The Netherlands, pp. 329–346.

Phillips, T.D., Afriyie-Gyawu, E., Williams, J., Huebner, H., Ankrah, N.A., Ofori-Adjei, D., Jolly, P., Johnson, N., Taylor, J., Marroquin-Cardona, A., Xu, L., Tang, L., Wang, J.S., 2008. Reducing human exposure to aflatoxin through the use of clay: a review. Food Addit. Contam. A-Chem. 25 (2), 134–145.

Smith, E.E., Phillips, T.D., Ellis, J.A., Harvey, R.B., Kubena, L.F., Thompson, J., Newton, G., 1994. Dietary hydrated sodium calcium aluminosilicate reduction of aflatoxin M1 residue in dairy goat milk and effects on milk production and components. J. Anim. Sci. 72 (3), 677–682.

Tenorio, A.M.G., Mulder, I., Dixon, J.B., 2008. Smectite clay adsorption of aflatoxin vs. octahedral composition as indicated by FTIR. Clays Clay Miner. 56 (5), 571–578.

Theng, B.K.G., 1974. The Chemistry of Clay-Organic Reactions. John Wiley and Sons, New York.

van Soest, T.C., Peerdeman, A.F., 1970a. The crystal structures of aflatoxin B_1. I. The structure of the chloroform solvate of aflatoxin B_1 and the absolute configuration of aflatoxin B_1. Acta Cryst. B26, 1940–1947.

van Soest, T.C., Peerdeman, A.F., 1970b. The crystal structures of aflatoxin B_1. II. The structure of an orthorhombic and a monoclinic modification. Acta Cryst. B26, 1947–1955.

Wang, P., Afriyie-Gyawu, E., Tang, Y., Johnson, N.M., Xu, L., Tang, L., Huebner, H.J., Ankrah, N.A., Ofori-Adjei, D., Ellis, W., Jolly, P.E., Williams, J.H., Wang, J.S., Phillips, T.D., 2008. NovaSil clay intervention in Ghanaians at high risk for aflatoxicosis: II. Reduction in biomarkers of aflatoxin exposure in blood and urine. Food Addit. Contam. A-Chem. 25 (5), 622–634.

Wicklein, B., Darder, M., Aranda, P., Ruiz-Hitzky, E., 2009. Phosphatidylcholine-clay systems as artificial lipid membrane supports of biological species. XIV International Clay Conference, Vol. I. Associazione Italiana per lo Studio delle Argille-onlus, Castellaneta Marina, Italy, p. 21.

Winfree, R.A., Allred, A., 1992. Bentonite reduces measurable aflatoxin b-1 in fish feed. Prog. Fish Cult. 54 (3), 157–162.

Computational evaluation of bonding between aflatoxin B_1 and smectite

Youjun Deng*,[a], Marek Szczerba[b]

[a]*Department of Soil and Crop Sciences, Texas A&M University College Station, TX 77843-2474*

[b]*Institute of Geological Sciences, Polish Academy of Sciences, Kraków Research Centre, ul. Senacka 1, 31-002 Kraków, Poland*

Abstract

Certain smectites can effectively adsorb aflatoxin B_1 but the interaction between the toxin and smectites is still poorly understood. The objective of this study was to computationally evaluate bonding mechanism between the adsorbed aflatoxin B_1 and smectite. Geometry optimization, net atomic charge distribution, vibration frequency and vibration intensity computation were performed for aflatoxin B_1 and cation-aflatoxin B_1 complexes. Molecular dynamics simulation was conducted for moist and dehydrated aflatoxin B_1-Na-Smectite complexes. The computed energies, net atomic charge distribution, and molecular dynamics simulations consistently revealed that the two carbonyl oxygens were the most important reacting sites with exchange cations and water in smectite interlayer. The two dihydrofuran oxygens had much less but still considerable contributions to the bonding. Substantial charge redistribution and bond elongation and shrinkage on the

*Corresponding author

Email addresses: yjd@tamu.edu (Youjun Deng), ndszczer@cyf-kr.edu.pl (Marek Szczerba)

carbonyl groups and adjacent bonds occurred with forming cation-aflatoxin B_1 complexes. The computed vibration frequency shifts and vibration intensity changes were in excellent agreement with experimental observations reported in the literature. The calculations confirmed the importance of carbonyl groups in the bonding of aflatoxin to smectite and revealed more subtle interactions between exchange cations and the dihydrofuran oxygens.

Keywords: aflatoxin B_1, smectite, bonding, simulation

1. Introduction

Aflatoxin B_1 (AfB_1) is a carcinogenic mycotoxin (Grant and Phillips, 1998) and can cause severe health problems and even death in animals and humans. Using smectite-rich clays to alleviate the toxicity of aflatoxins has been tested for more than 30 years by animal scientists and toxicologists in many countries (e.g., Masimango et al., 1978, 1979; Phillips et al., 1988; Nahm, 1995; Márquez and Hernandez, 1995; Chaturvedi and Singh, 2002; Chaturvedi et al., 2002; Desheng et al., 2005; Magnoli et al., 2008a,b; Wang et al., 2008; Afriyie-Gyawu et al., 2008a,b; Phillips et al., 2008). The effectiveness of the clay(s) has been demonstrated by these animal feed experiments and human clinical trials.

To understand reactions between the toxins and the clays so other reac-

22 tive clays can be selected or the less effective clays can be improved, several
23 groups explored the thermodynamics of the adsorption, mineralogical cri-
24 teria, and bonding mechanism between AfB_1 and smectites (Kannewischer
25 et al., 2006; Dixon et al., 2008; Mulder et al., 2008; Tenorio et al., 2008; Deng
26 et al., 2010). Deng et al. (2010) claimed that AfB_1 could occupy the inter-
27 layer space of smectites, and the major bonding mechanisms between AfB_1
28 molecules and dry smectite were ion-dipole interactions/coordination be-
29 tween the two carbonyl groups and the exchange cations, and H-bonding be-
30 tween the carbonyl groups with water in the hydration shell of the exchange
31 cations when the smectite was wet. There were several other proposed bond-
32 ing models, such as electron donor-acceptor model (Phillips, 1999; Phillips
33 et al., 2006, 2008), chelating of the two carbonyl groups with uncoordinated
34 edge aluminum (Phillips et al., 1994), and hydrogen bonding on smectite
35 edge (Desheng et al., 2005), and bonding with the expoxidazed C10=C11
36 (Fig. 1) (Tenorio et al., 2008). Which bonding mechanism is the dominated
37 one in the adsorption of aflatoxin by smectite?

38 In the adsorption of simple O-containing organic compounds such as
39 aldehydes, ketones, alcohols, ethers, amides, carboxylic acid to smectite,
40 it is the oxygen atoms that play the critical roles in the bonding through
41 ion-dipole interaction or H-bonding (Theng, 1974). The importance of the

carbonyl oxygens of AfB_1 in the bonding was realized by several researchers (e.g., Phillips et al., 1994; Deng et al., 2010). There are six oxygen atoms in an AfB_1 molecule (Fig. 1), the role of other non-carbonyl oxygens at positions 9, 12, 13, and 17 in AfB_1 cannot be judged unambiguously based on infrared spectroscopic data due to overlap of the infrared bands. There are several possible positions for the exchange cation to react with the oxygens individually or simultaneously as shown in Fig. 1. The objectives of this study were (1) to computationally evaluate the adsorption models of AfB_1-smectite complexes and (2) to refine the bonding mechanism between AfB_1 and smectite.

2. Molecular simulations

2.1. Molecular geometry and vibrational bands

Molecular geometry optimization of AfB_1 molecules were performed with Density Functional Theory (DFT) at PCM/B3LYP/DGDZVP level of theory (Miertus et al., 1981; Lee et al., 1988; Becke, 1993) using Gaussian Inc. software (Frisch et al., 2004). The distribution of Mulliken atomic charges, vibration frequencies, and vibration intensities were computed after AfB_1 and the proposed cation-AfB_1 complex structures were optimized. Surface electrostatic potential map of AfB_1 was created with software VEGA ZZ

(Pedretti et al., 2004). Potential Energy Distributions (PED) of vibrational bands of AfB_1 and cation-AfB_1 complexes were calculated with software GAR2PED (Martin and Van Alsenoy, 1995). The calculated frequencies, intensities, and PED of vibrational fundamentals of AfB_1 and K-, Na-, Ca-, Mg-, and Mn-AfB_1 complexes were tabulated and are available from the authors upon request.

2.2. Molecular dynamics

Molecular dynamics of moist and dehydrated aflatoxin B_1-Na-smectite (AfB_1-Na-Sm) complexes at constant pressure and temperature (NPT) ensemble was simulated with program DLPOLY 2 (Smith and Forester, 1996). The simulation included two layers of smectite consisted of 64 unit cells (8a×4b×2c, 2560 structural atoms). A half charge per half unit cell was assumed for the smectite model $[Na_{0.5}(Al_{1.5}Mg_{0.5})Si_4O_{10}(OH)_2]$. Eleven aflatoxin B_1 molecules $[C_{17}H_{12}O_6]$ and 32 Na^+ ions were included in each of the two interlayer spaces. The number of interlayer aflatoxin molecules was based on the maximum adsorption capacity (14% of smectite's mass) determined from adsorption isotherm (Deng et al., 2010). To simulate the moist complex, a total of 255 water molecules (about 10% of smectite mass) were introduced into the two interlayer spaces. The charge and potential for water were taken from the SPC-E model (Berendsen et al., 1987), for AfB_1

from the OPLS-AA force field (e.g., Jorgensen et al., 1996), and for smectite and exchange Na^+ from the CLAYFF force field (Cygan et al., 2004). Interactions among water molecules, AfB_1, and the mineral surface were calculated using the standard Lorentz-Berthelot mixing rules (e.g., Cygan et al., 2004). A 50,000-step molecular dynamics simulation at 298 K was carried out for a 50-picosecond (ps) period with a time step of 0.001 ps. The last 10,000 steps were used in the analysis of radial distribution functions.

The optimized basal spacing from the molecular dynamic simulation was compared with that of AfB_1-Na-Sm complex synthesized by Deng et al. (2010). The basal spacing of the synthetical AfB_1-Na-Sm complex was measured with X-ray diffraction at 30 °C and 0% (nitrogen purge), 51% (room humidity), and 100% humidity in a reaction chamber described by Deng et al. (2010).

3. Results and Discussion

3.1. Molecular configuration and energy

Our optimized aflatoxin B_1 configuration (Fig. 2b) was nearly identical to those measured experimentally (van Soest and Peerdeman, 1970; van Soest and Peerdeman, 1970) and calculated theoretically (Billes et al., 2006). The molecule had a coplanar configuration of which the B, C, D, and E rings, two

carbonyl groups, and the methoxy group lay in one plane. The dihydrofuran ring A protruded toward the viewer in Figs. 1 and 2. The methoxy group was repulsed from hydrogen atoms H33 and H34 of ring E.

Energy calculation after configuration optimization suggested that interactions of both Na^+ and Mn^{2+} with the two carbonyl oxygens at position *a* (Fig. 1) resulted in the lowest energy compared to the interactions at positions *b* and *c*. More than 96% of interactions between the exchange cations would occur with the two carbonyl oxygens at position *a*, and a small portion of the interactions might occur with the dihydrofuran oxygens (Table 1).

3.2. Charge distribution and surface electrostatic potential of aflatoxin B_1

The most negative charge (-0.609 atomic charge units) in AfB_1 was on the C2 atom and the most positive charge (+0.417 atomic charge units) was on the C1 atom of the benzene ring (Fig. 2a). The surface electrostatic potential at those sites (Fig. 2b), however, were not at the extremes due to the opposite charge from their neighboring hydrogen or oxygen atoms. The two carbonyl oxygens were both moderately negative and their surface electrostatic potential was the most negative (-0.22 atomic charge units). Surface electrostatic potential at sites near the two dihydrofuran oxygens was less negative (about -0.1 atomic charge units). The most positive surface electrostatic potential was on the methyl group (CH_3). The calculated

surface electrostatic potential was consistent with the AfB_1 crystal structure determined by X-ray diffraction (van Soest and Peerdeman, 1970; van Soest and Peerdeman, 1970): two AfB_1 molecules were linked together by H-bonds between the carbonyl oxygens of one molecule and the other's methyl group. The surface electrostatic distribution indicated that the two carbonyl oxygens were the most important reaction sites when AfB_1 coordinated with the positively charged exchange cations in smectite. The two dihydrofuran oxygens (position *c* in Fig. 1) were next possible reacting sites for the exchange cations.

3.3. Molecular dynamics simulation

The molecular dynamics simulation of dehydrated AfB_1-Na-Sm complex revealed that the exchange Na^+ cations migrated to the basal surfaces of smectite whereas AfB_1 molecules remained in the centers of the interlayer spaces (Fig. 3, a1). The major plane of AfB_1 lay parallel to the smectite basal surfaces. The dehydrated AfB_1-Na-Sm complex had a 1.33 nm basal spacing, which was close to the experimentally measured value of 1.28 nm from the synthetical AfB_1-Na-Sm complex at 0% humidity. The minor difference was likely due to incomplete saturation of AfB_1 in the synthesized complex. In the moist AfB_1-Na-Sm complex, the major plane of AfB_1 slightly tilted toward smectite basal surfaces (Fig. 3, b1). Water filled space between

Na^+ ions, AfB_1, and smectite surfaces. The simulated moist AfB_1-Na-Sm complex was expanded to a 1.52 nm in basal spacing. Experimental measurements of the synthesized AfB_1-Na-Sm complex had a basal spacing of 1.3 nm at 51% humidity and of a more varied 1.4-16 nm at nearly 100% humidity. The assumed 10% (mass) moist content in the computation was probably equivalent to a humidity close to 100%.

The molecular dynamics simulation showed that the carbonyl oxygens closely approached the exchange Na^+ ions (the A1 and A2 types in Fig. 3, a2). Most of the AfB_1 molecules interacted with the exchange cations by docking one exchange cation into two carbonyl oxygens (the A1 type), a few of them through individual interaction between one of the two carbonyl oxygen with one cation (the A2 type). The molecular dynamics simulation also suggested that some dihydrofuran oxygens were in close proximity to the exchange cations (the C type). Interactions between Na^+ and other AfB_1 oxygen atoms (e.g., the B type) were of much less importance. In the moist AfB_1-Na-Sm complex (Fig. 3, b2), all above bonding types were observed. Moreover, interactions between the AfB_1 oxygens and water molecules (H bonding) were common. Many of the carbonyl oxygens and dihydrofuran oxygens were in direct contacts with both water molecules and Na^+ ions. All Na^+ ions were surrounded by different numbers of water molecules.

The radial distribution functions offered a more quantitative estimation of the bonding probability. In the dehydrated AfB_1-Na-Sm complex, the Na^+ ions were coordinated mainly to the carbonyl oxygens with a bond length of 2.3 Å (Fig. 4a, solid line). Direct interactions between Na^+ ions and the dihydrofuran oxygens with an average bond length of 2.4 Å were also important (Fig. 4a, dashed line). In the moist AfB_1-Na-Sm complex, the Na^+ ions were mainly bonded to water molecules (Fig. 4b, dashed grey line), which suggested that hydration of the cations expelled AfB_1 molecules from Na^+ ions. The carbonyl oxygens, however, also had nearly the same probability as water to coordinate to Na^+ ions (Fig. 4b, solid line). In both dehydrated and moist AfB_1-Na-Sm complexes, the dihydrofuran oxygens had nearly 50% probabilities as carbonyl oxygens to bond to Na^+ ions. Interactions of Na^+ ions with other oxygens (O13 and O17) were negligible in both complexes (Fig. 4a and b, dotted lines). The water hydrogen to AfB_1 radial distribution functions (Fig. 4c) suggested that the carbonyl oxygens also had higher probability than other oxygens to form H-bonds with water in the moist AfB_1-Na-Sm complex.

The molecular dynamics simulation suggested that the carbonyl groups would be the major functional groups in the coordination between exchange cations and AfB_1 molecules. The dihydrofuran oxygens also would con-

tribute to the bonding with less importance. The presence of water molecules would compete with AfB_1 molecules for the exchange cations, but they would not be able to diminish the direct bonding between exchange cations and the AfB_1 molecules at the tested moisture content (about 10% by mass). The Na-oxygen radial distribution functions (Fig. 4, a and b) suggested that the bonding strength between smectite and AfB_1 should be affected by the type of exchange cations in both dehydrated and moist (or not fully dehydrated) AfB_1-Na-Sm complexes. The infrared bands of adsorbed AfB_1 should shift when Na was replaced by other cations. The predicted shifts were indeed observed when the AfB_1-Na-Sm was saturated with Ca, Mg, La, Al, Cu, Mn, and Ni cations in the experiment of Deng et al. (2010).

3.4. Charge redistribution and configuration changes of AfB_1 after interacting with different exchange cations

When exchange cations interacted with the two carbonyl oxygens of an AfB_1 molecule, the main bonding would be ion-dipole interaction for alkali cations and alkaline earth cations as well as coordination for transition cations. The interactions were stronger for the divalent cations than for the monovalent cations. The calculation revealed that, after interacting with the AfB_1 molecules, exchange cations possessed less positive charge than their ideal valences indicated. This meant that electrons shifted from AfB_1

molecule toward the exchange cations. Bonding between the exchange cation and carbonyl oxygens led to substantial charge redistribution on atoms in AfB_1: atoms that were directly involved in the bonding i.e., O18 and O22, and their immediate neighboring C16 and C21 of carbonyl groups had the greatest changes with a magnitude of 0.1-0.2 atomic charge units (Fig. 5). The carbonyl oxygens became more negative and the carbons became more positive. The magnitude of these changes increased when the ion-dipole interaction/coordination was enhanced by increasing cation valence, reducing ion radius, or introducing a transition heavy metal cation. The net charge distribution suggested that electrons were shifted from C16 and C21 to O18, O22 and C15. The changes in charges propagated to other parts of AfB_1 molecule with decreasing magnitudes.

When ion-dipole interaction or coordination occurred between the two carbonyl groups and the cations, the basic co-planar AfB_1 molecular configuration was well preserved. The cations fell in the same plane. When the valence/radius ratio of the cation was increased, the distances between the carbonyl groups and the cations were reduced: a nearly 0.8 Å reduction was observed in the distance between carbonyl oxygens and the cation when K^+ was replaced by Mg^{2+}, which suggested an increasing ion-dipole interaction. Transition metal Mn^{2+} was slightly more distant from the car-

bonyl groups than Mg^{2+}. With increasing cation charge/radius ratio, the neighboring bonds shrank and expanded alternatively (Fig. 6): the greatest elongations occurred on the two carbonyl groups (C16O18 and C21O22), and the greatest shrinkage occurred on their immediately adjacent bonds O17C16, C21C15, and C16C15. The alternative elongation/shrinkage propagated to rings C, B, and A with reducing amplitudes.

3.5. Computed vibrational band positions and intensities

When exchange cations interacted with AfB_1 at position *a* as shown in Fig. 1, several AfB_1 infrared band positions shifted and band intensity changed substantially. The greatest changes were observed on the carbonyl bonds and their adjacent bonds. Both in-phase and opposite-phase stretching vibrations of the two carbonyl bonds (Figs. 7A and 7B) shifted to lower frequencies (Figs. 8A and 8B). When the AfB_1 was bonded to Mn^{2+}, a 60 cm^{-1} red shift was observed on the in-phase stretching vibration (Fig. 8A) and a 112 cm^{-1} red shift was observed on the opposite-phase stretching vibrations (Fig. 8B). These shifts suggested substantial weakening of the carbonyl bonds after coordinating to Mn^{2+}. The calculation also indicated that band intensities of opposite-phase stretching vibrations (Fig. 8B) of the two carbonyl groups were much weaker than their nearby bands, which may hinder the experimental observation of the shifts. Smaller red shifts were

observed on vibrations that had less contributions from stretching vibrations of the carbonyl bonds (Figs. 7C, 7D, 8C, and 8D). The greatest shift, which was 13 cm^{-1} only, of these bands occurred still in Mn^{2+}-AfB_1 complex.

Several bands that contained the bending vibrations of the carbonyl bonds had blue shifts (Figs. 7E-7I). The greatest blue shift was observed on the in-plane, symmetric swing vibrations of the two carbonyl groups (Fig. 7G). Interacting with Mg^{2+} resulted in the greatest blue shift of 67 cm^{-1} (Fig. 9G). Vibration E, F, H, and I in Fig. 7 were mainly due to deformation of ring C, D, or E but much less from bending vibrations of the carbonyl bonds. These bands shifted less compared to band G.

After interacting with different cations, substantial changes in the potential energy distribution also occurred. For example, along the red shifts of the characteristic in-phase carbonyl stretching vibration, deformational in-plane-bending of rings D and E made greater contribution to this vibration, especially for the stronger ion-dipole interaction/coordination with the divalent cations.

There were no significant changes in band positions or intensities in the 3000–3300 cm^{-1} range (data not shown) in which various C-H stretching vibrations occurred. Most bands in the range 450–800 cm^{-1} did not show more than 10 cm^{-1} shifts (data not shown). When AfB_1 reacted with the

cations, significant but not systematic changes in potential energy distributions were observed on the <450 cm^{-1} bands (data not shown). The nonsystematic changes in potential energy distributions resulted in very different low-frequency deformation vibrations that could not be compared directly among the studied five cations.

3.6. Comparison between calculated and the published experimental infrared spectra of AfB_1-smectite complexes

The computed infrared band shifts were in excellent agreement with the experimental spectra reported by Deng et al. (2010). Like most vibration frequency computation, the computed frequencies were higher than the experimental observations. This was partially due to the omission of the effects of moisture and smectite on AfB_1. Yet, the directions and magnitudes of the calculated AfB_1 infrared band shifts were consistent with the experimental observations. When the infrared spectra were recorded at nearly 0% humidity, the in-phase stretching vibrations of the two carbonyl bonds (Fig. 7A) in the AfB_1-smectite complexes red shifted in increasing magnitudes in the order of K<Na<Ca<Mg<Mn. The experimentally recorded frequency (1705 cm^{-1}) of the AfB_1-Mn-Sm was 31 cm^{-1} lower than that of the AfB_1-K-Sm. Only a shoulder at 1657 cm^{-1} was observed on the infrared spectrum of AfB_1-K-Sm, and this shoulder was attributed to the

opposite phase vibrations of the carbonyl groups (Fig. 7B). It was believed that this band was fused to the more intense bands at 1630 cm^{-1} in other cation saturated AfB_1-Sm complexes (Deng et al., 2010). This assignment agreed with the computed weak intensity of the opposite-phase stretching vibrations of carbonyl groups (Fig. 8B). It could be shaded by other nearby strong bands at about 1654 cm^{-1} and 1614 cm^{-1}, which were mainly due to the in-plane deformations of benzene ring C (Fig. 8). The experimentally observed strong band at 1630 cm^{-1} must be corresponding to the computed 1654 cm^{-1} band in Fig. 8 due to the same characteristics in intensity and inertness to cation exchange. Small red shifts were observed on the poorly-resolved band at 1590 cm^{-1} on the experimental infrared spectra, this band must be corresponding to the computed 1616 cm^{-1} band (Fig. 8C). On the experimental spectra, a 12 cm^{-1} red shift was observed from the highest frequency of 1550 cm^{-1} in AfB_1-K-Sm to 1538 cm^{-1} in AfB_1-Mn-Sm. This band must be corresponding to the computed 1564 cm^{-1} band (Fig. 8D). On the experimental spectra, there was a more than 16 cm^{-1} blue shift from the 1496 cm^{-1} band in AfB_1-K-Sm to 1512 cm^{-1} in AfB_1-Mn-Sm (Deng et al., 2010). These bands must be corresponding to the computed E bands in Fig. 8. Minor blue shift was observed on the experimental 1444 cm^{-1} band, which was believed as the the computed F bands.

On the experimental spectra, there were several bands at 1208, 1246, 1273, 1304, and 1343 cm^{-1} did not show distinct changes after cation exchange (Deng et al., 2010). Experimental spectra also did not show distinct changes in the C-H bands after cation exchange. These observations were in agreement with the computation. On the experimental spectra, the strong infrared absorption from smectite hindered the measurements of AfB_1 bands in the <1200 cm^{-1} range and therefore, the computation for those bands could not be evaluated experimentally.

4. Conclusions

Molecular geometry optimization, energy minimization, surface electrostatic potential calculation, and molecular dynamics simulation consistently suggested that the two carbonyl oxygens on the AfB_1 molecules played the most important role in the bonding of the toxin to smectite through ion-dipole interaction/coordination under fully and partially dehydrated conditions. The computed infrared band shifts and intensity changes of such bonding with different cations (K, Na, Ca, Mg, and Mn) were in excellent agreement with the reported infrared spectra recorded at 0% humidity reported in the literature. The computations further indicated the bonding was mainly between the two carbonyl oxygens and exchanges cations

in the interlayer of smectite. The dihydrofuran oxygens might be involved in the bonding between AfB_1 and exchange cations in smectite, but this interaction contributed less in the adsorption of AfB_1. This improved understanding about the bonding mechanism offered important guidance for future smectite selection and modification to achieve high selectivity and high adsorption capacity in binding AfB_1.

5. Acknowledgements

Funding was partially supplied by the Texas AgrilLife Research, Texas Corn Producers Board, and National Corn Growers Association (USA).

References

Afriyie-Gyawu, E., Ankrah, N. A., Huebner, H. J., Ofosuhene, M., Kumi, J., Johnson, N. M., Tang, L., Xu, L., Jolly, P. E., Ellis, W. O., Ofori-Adjei, D., Williams, J. H., Wang, J. S., Phillips, T. D., 2008a. NovaSil clay intervention in Ghanaians at high risk for aflatoxicosis. I. Study design and clinical outcomes. Food Addit. Contam. Part A-Chem. 25 (1), 76–87.

Afriyie-Gyawu, E., Wang, Z., Ankrah, N. A., Xu, L., Johnson, N. M., Tang, L., Guan, H., Huebner, H. J., Jolly, P. E., Ellis, W. O., Taylor, R., Brattin, B., Ofori-Adjei, D., Williams, J. H., Wang, J. S., Phillips, T. D.,

2008b. NovaSil clay does not affect the concentrations of vitamins A and E and nutrient minerals in serum samples from Ghanaians at high risk for aflatoxicosis. Food Addit. Contam. Part A-Chem. 25 (7), 872–884.

Becke, A. D., 1993. Density-functional thermochemistry. III. The role of exact exchange. J. Chem. Phys. 98 (7), 5648–3652.

Berendsen, H. J. C., Grigera, J. R., Straatsma, T. P., 1987. The missing term in effective pair potentials. J. Phys. Chem. 91 (24), 6269–71.

Billes, F., Móricz, A. M., Tyihák, E., Mikosch, H., 2006. Simulated vibrational spectra of aflatoxins and their demethylated products and the estimation of the energies of the demethylation reactions. Spectrochim. Acta A 64 (3), 600–622.

Chaturvedi, V. B., Singh, K. S., 2002. Detoxification of aflatoxin by adsorbents. Indian J. Anim. Sci. 72 (10), 924–927.

Chaturvedi, V. B., Singh, K. S., Agnihotri, A. K., 2002. In vitro aflatoxin adsorption capacity of some indigenous aflatoxin adsorbents. Indian J. Anim. Sci. 72 (3), 257–260.

Cygan, R. T., Liang, J.-J., Kalinichev, A. G., 2004. Molecular models of hy-

droxide, oxyhydroxide, and clay phases and the development of a general force field. J. Phys. Chem. B 108 (4), 1255–1266.

Deng, Y., Barrientos Velazquez, A. L., Billes, F., Dixon, J. B., 2010. Bonding mechanisms between aflatoxin B_1 and smectite. Appl. Clay Sci. 50 (1), 92–98.

Desheng, Q., Fan, L., Yanhu, Y., Niya, Z., 2005. Adsorption of aflatoxin B-1 on montmorillonite. Poult. Sci. 84 (6), 959–961.

Dixon, J. B., Kannewischer, I., Tenorio Arvide, M. G., Barrientos Velazquez, A. L., 2008. Aflatoxin sequestration in animal feeds by quality-labeled smectite clays: an introductory plan. Appl. Clay Sci. 40, 201–208.

Frisch, M., Trucks, G., Schlegel, H., Scuseria, G., Robb, M., Cheeseman, J., Montgomery, J., Vreven, J., Kudin, K., Burant, J., Millam, J., Iyengar, S., Tomasi, J., Barone, V., Mannucci, B., Cossi, M., Scalmani, G., Rega, N., Petersson, G., Nakatsuji, H., Hada, M., Ehara, M., Toyota, K., Fukuda, F., Hasegawa, J., Ishida, M., Nakajima, T., Honda, Y., Kitao, O., Nakai, H., Klene, M., Li, X., Knox, J., Hratchian, H., Cross, J., Bakken, V., Adamo, C., Jramillo, J., Gomperts, R., Stratmann, R., Yazyev, O., Austin, A., Cammi, R., Pomelli, C., Ochterski, J., Ayala, P., Morokuma, K., Voth, G., Salvador, P., Dannenberg, J., Zakrzewski, V., Dapprich, S.,

373 Daniels, A., Strain, M., Frakas, O., Malick, D., Rabuck, A., Raghavachari,
374 K., Foresman, J., Ortiz, J., Cui, Q., Baboul, A., Clifford, S., Cislowski, J.,
375 Stefanov, B., Liu, G., Liashenko, A., Piskorz, P., Komaromi, I., Martin,
376 R., Fox, D., Keith, T., Al-Laham, M., Peng, C., Nanayakkara, A., Chal-
377 lacombe, M., Gill, P., Johnson, B., Chen, W., Wong, M., Gonzalez, C.,
378 Pople, J., 2004. Gaussian-94, Revision, C.3,. Gaussian, Inc., Pittsburgh,
379 PA.

380 Grant, P. G., Phillips, T. D., 1998. Isothermal adsorption of aflatoxin B_1 on
381 HSCAS clay. J. Agric. Food Chem. 46 (2), 599–605.

382 Jorgensen, W. L., Maxwell, D. S., Tirado-Rives, J., 1996. Development and
383 testing of the OPLS all-atom force field on conformational energetics and
384 properties of organic liquids. J. Am. Chem. Soc. 118 (45), 11225–11236.

385 Kannewischer, I., Tenorio, A. M. G., White, G. N., Dixon, J. B., 2006. Smec-
386 tite clays as adsorbents of aflatoxin B1: Initial steps. Clay Sci. 12 (Sup-
387 plement 2), 199–204.

388 Lee, C., Yang, W., Parr, R. G., 1988. Development of the Colle-Salvetti
389 correlation-energy formula into a functional of the electron density. Phys.
390 Rev. B: Condens. Matter 37 (2), 785–759.

391 Magnoli, A. P., Cabaglieri, L. R., Magnoli, C. E., Monge, J. C., Miazzo,

R. D., Peralta, M. F., Salvano, M. A., Rosa, C. A. R., Dalcero, A. M., Chiacchiera, S. M., 2008a. Bentonite performance on broiler chickens fed with diets containing natural levels of aflatoxin B_1. Rev. Bras. Med. Vet 30 (1), 55–60.

Magnoli, A. P., Tallone, L., Rosa, C. A. R., Dalcero, A. M., Chiacchiera, S. M., Torres Sanchez, R. M., 2008b. Commercial bentonites as detoxifier of broiler feed contaminated with aflatoxin. Appl. Clay Sci. 40 (1-4), 63–71.

Márquez, R. N., Hernandez, I. T. D., 1995. Aflatoxin adsorbent capacity of two Mexican aluminosilicates in experimentally contaminated chick diets. Food Addit. Contam. 1995, 431–433.

Martin, J. M. L., Van Alsenoy, C., 1995. GAR2PED. University of Antwerp.

Masimango, N., Remacle, J., Ramaut, J., 1979. Elimination of aflatoxin B1 from contaminated media by swollen clays. Ann. Nutr. Aliment. 33 (1), 137–1–47.

Masimango, N., Remacle, J., Ramaut, J. L., 1978. The role of adsorption in the elimination of aflatoxin B1 from contaminated media. Eur. J. Appl. Microbiol. Biotechnol. 6 (1), 101–105.

Miertus, S., Scrocco, E., Tomasi, J., 1981. Electrostatic interaction of a solute with a continuum. A direct utilization of ab initio molecular potentials for the prevision of solvent effects. Chem. Phys. 55 (1), 117–129.

Mortland, M. M., 1970. Clay-organic complexes and interactions. Adv. Agron. 22, 75–117.

Mortland, M. M., 1986. Mechanisms of adsorption of nonhumic organic species by clays. In: Huang, P., Schnitzer, M. (Eds.), Interactions of Soil Minerals with Natural Organics and Microbes. Vol. 17 of SSSA Special Publication. Soil Science Society of America, Inc., Madison, Wisconsin, pp. 59–76.

Mulder, I., Tenorio Arvide, M. G., White, G. N., Dixon, J. B., 2008. Smectite clay sequestration of aflatoxin B1: Mineral dispersivity and morphology. Clays Clay Miner. 56, 559–571.

Nahm, K. H., 1995. Prevention of aflatoxicosis by addition of antioxidants and hydrated sodium calcium aluminosilicate to the diet of young chicks. Nippon Kakin Gakkaishi 32 (2), 117–127.

Pedretti, A., Villa, L., Vistoli, G., 2004. VEGA - An open platform to develop chemo-bio-informatics applications, using plug-in architecture and script programming. J. Comput. Aided. Mol. Des. 18 (3), 167–173.

429 Phillips, T. D., 1999. Dietary clay in the chemoprevention of aflatoxin-
430 induced disease. Toxicol. Sci. 52 (2), 118–126.

431 Phillips, T. D., Afriyie-Gyawu, E., Wang, J. S., Williams, J. O., Huebner,
432 H., 2006. The potential of aflatoxin sequestering clay. In: Barug, D., Bhat-
433 nagar, D., van Egmond, H. P., van Der Kamp, J. W., van Osenbruggen,
434 W. A., Visconti, A. (Eds.), The Mycotoxin Factbook: Food and Feed Top-
435 ics. Wageningen Academic Publishers, Wageningen, The Netherlands, pp.
436 329–346.

437 Phillips, T. D., Afriyie-Gyawu, E., Williams, J., Huebner, H., Ankrah, N. A.,
438 Ofori-Adjei, D., Jolly, P., Johnson, N., Taylor, J., Marroquin-Cardona, A.,
439 Xu, L., Tang, L., Wang, J. S., 2008. Reducing human exposure to aflatoxin
440 through the use of clay: A review. Food Addit. Contam. Part A-Chem.
441 25 (2), 134–145.

442 Phillips, T. D., Clement, B. A., Park, D. L., 1994. Approaches to reduc-
443 tion of aflatoxins in foods and feeds. In: Eaton, D. L., Groopman, J. D.
444 (Eds.), The Toxicology of Aflatoxins: Human Health, Veterinary, and
445 Agricultural Significance. Academic Press, San Diego, pp. 383–406.

446 Phillips, T. D., Kubena, L. F., Harvey, R. B., Taylor, D. R., Heidelbaugh,

N. D., 1988. Hydrated sodium calcium aluminosilicate: A high affinity sorbent for aflatoxin. Poult. Sci. 67, 243–247.

Smith, W., Forester, T. R., 1996. DL-POLY _2.0: a general-purpose parallel molecular dynamics simulation package. J. Mol. Graphics 14 (3), 136–141.

Tenorio, A. M. G., Mulder, I., Dixon, J. B., 2008. Smectite clay adsorption of aflatoxin vs. octahedral composition as indicated by FTIR. Clays Clay Miner. 56 (5), 571–578.

Theng, B. K. G., 1974. The Chemistry of Clay-Organic Reactions. John Wiley and Sons, New York.

van Soest, T. C., Peerdeman, A. F., 1970. The crystal structures of aflatoxin B_1. I. The structure of the chloroform solvate of aflatoxin B_1 and the absolute configuration of aflatoxin B_1. Acta Cryst. B26, 1940–1947.

van Soest, T. C., Peerdeman, A. F., 1970. The crystal structures of aflatoxin B_1. II.The structure of an orthorhombic and a monoclinic modification. Acta Cryst. B26, 1947–1955.

Wang, P., Afriyie-Gyawu, E., Tang, Y., Johnson, N. M., Xu, L., Tang, L., Huebner, H. J., Ankrah, N. A., Ofori-Adjei, D., Ellis, W., Jolly, P. E., Williams, J. H., Wang, J. S., Phillips, T. D., 2008. NovaSil clay interven-

tion in Ghanaians at high risk for aflatoxicosis: II. Reduction in biomarkers of aflatoxin exposure in blood and urine. Food Addit. Contam. Part A-Chem. 25 (5), 622–634.

Table 1: Energy analysis of Na- and Mn-AfB_1 complexes coordinated at positions *a*, *b*, and *c* as shown in Fig. 1.

		PCM* energy (kcal/mol)		Portion (%) at
Cation	Position	Absolute	Relative	equilibrium
Na	a	-796163.7	0.0	96.3
	b	-796157.0	6.7	0.4
	c	-796159.7	4.0	3.3
Mn	a	-1416390.9	0.0	99.8
	b	-1416369.3	21.6	0.0
	c	-1416383.2	7.7	0.2

*PCM: polarizable continuum model

List of Figures

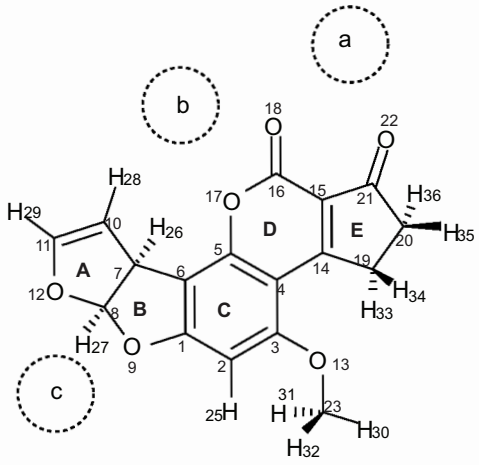

Figure 1: Likely positions (a, b, and c) for exchange cations to interact with an AfB_1 in smectite.

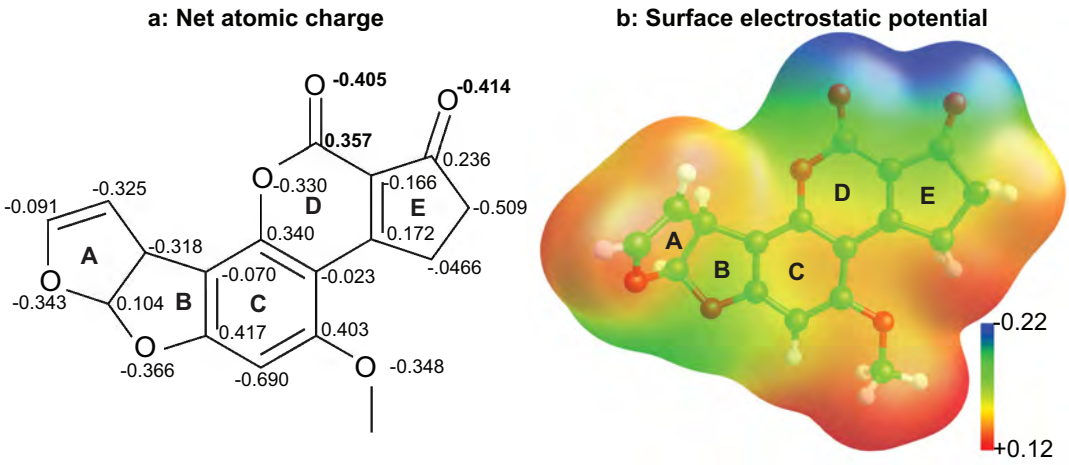

Figure 2: Net atomic charge (a) of non-hydrogen atoms and surface electrostatic potential (b) of AfB_1. Unit: elementary charge.

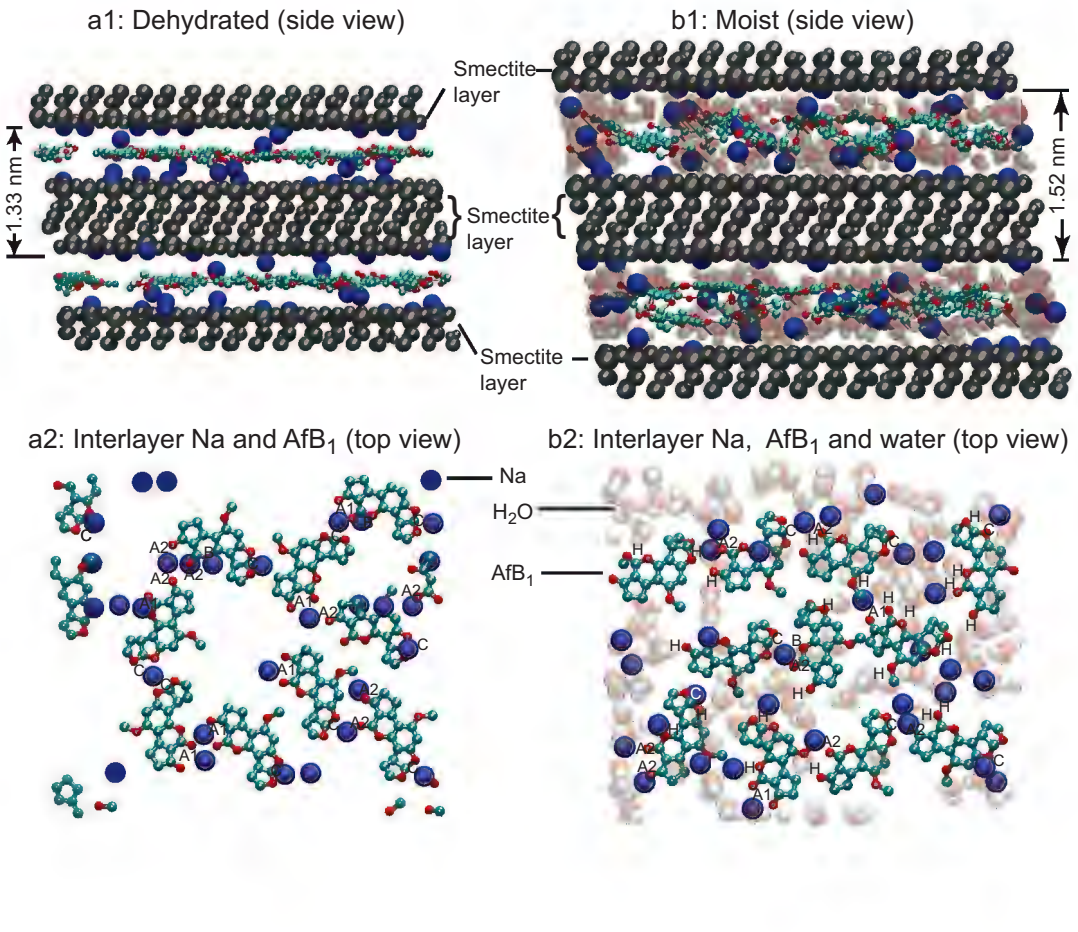

Figure 3: Optimized structures from molecular dynamics simulation of dehydrated (a1 and a2) and moist (b1 and b2) AfB_1-Na-smectite complexes. Top images are side views of the complexes and bottom images are top views of the interlayer Na, AfB_1 and water molecules.

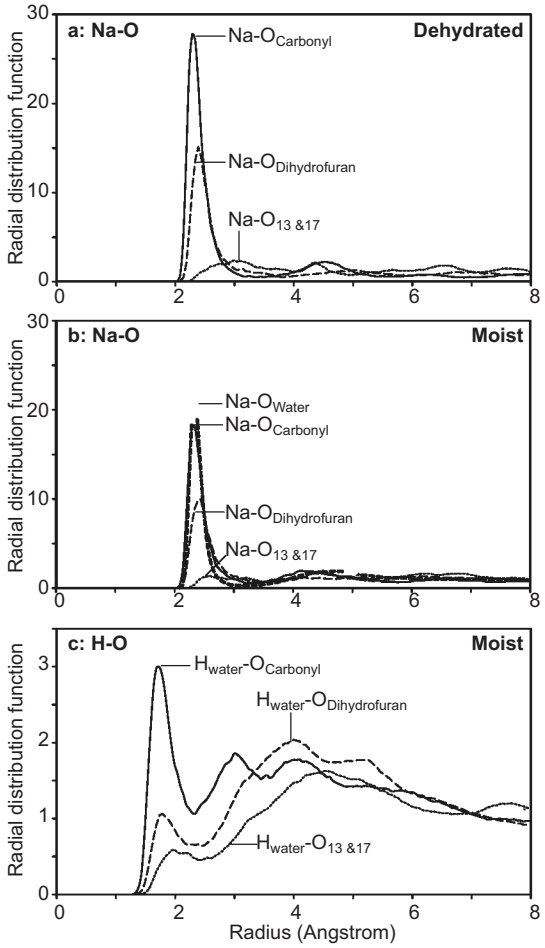

Figure 4: Radial distribution functions of interlayer sodium ions (a and b) to oxygen atoms in AfB_1 and water molecules, and of water hydrogens (c) to AfB_1 oxygens based on the last 10,000 step molecular dynamics simulations of the AfB_1-Na-smectite complexes.

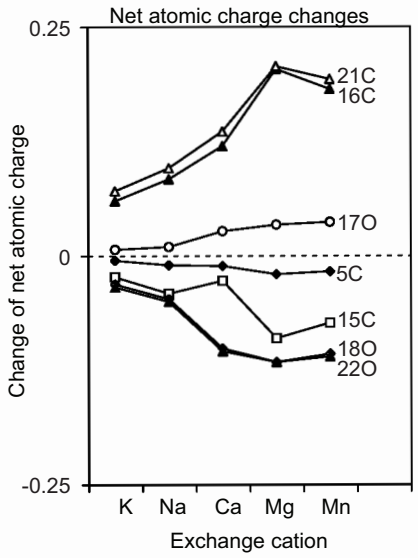

Figure 5: Net atomic charge changes in AfB_1 molecules coordinated to different exchange cations through the two carbonyl oxygens. Other atoms had less changes in net charge than the atoms shown in the figure.

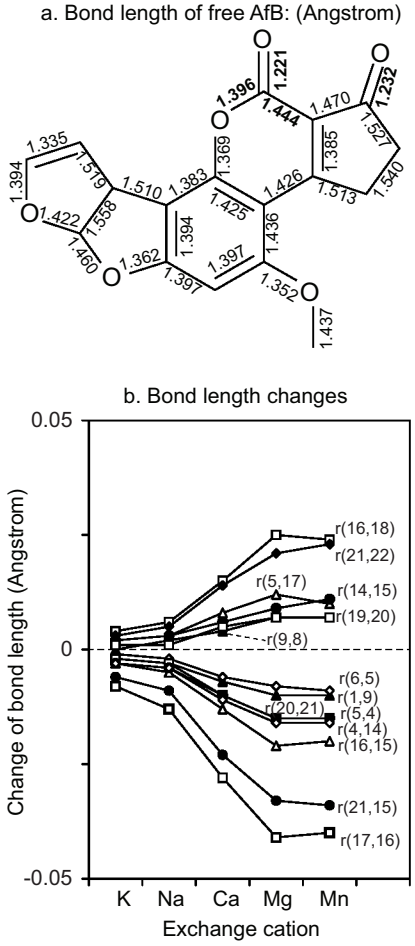

Figure 6: Bond lengthes of free AfB_1 (a) and their changes in AfB_1 molecules coordinated to different exchange cations through the two carbonyl oxygens (b). Other bonds had less changes than the bonds shown in the figure.

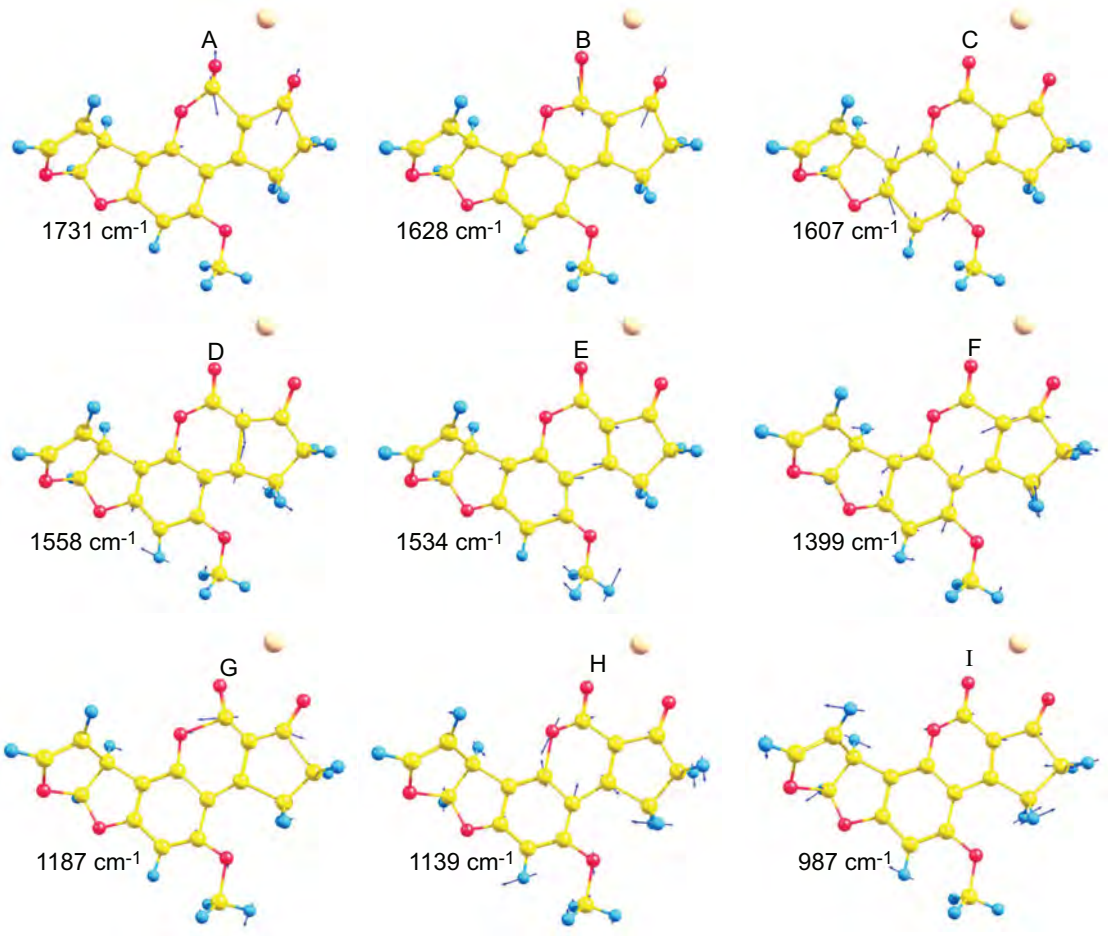

Figure 7: Example Ca-AfB$_1$ molecular vibrations and their corresponding frequencies. The arrow axes represent the vibration directions and arrow lengths were proportional to the vibration amplitudes.

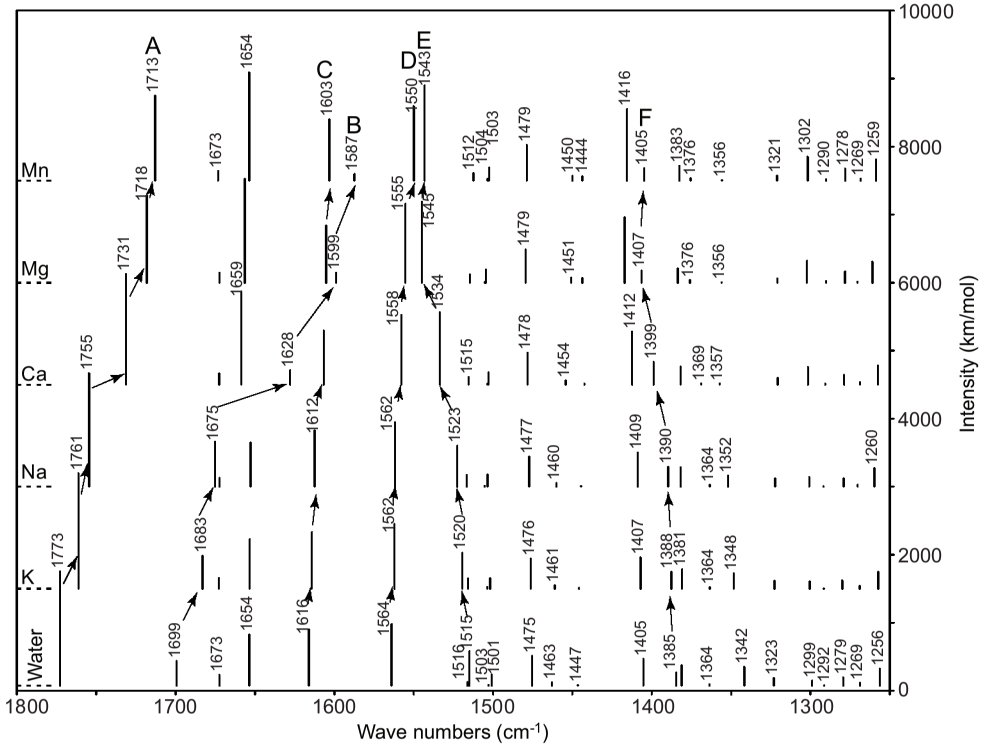

Figure 8: Calculated infrared bands of AfB_1 and AfB_1-Metal complexes in the range of 1250 to 1800 cm^{-1}.

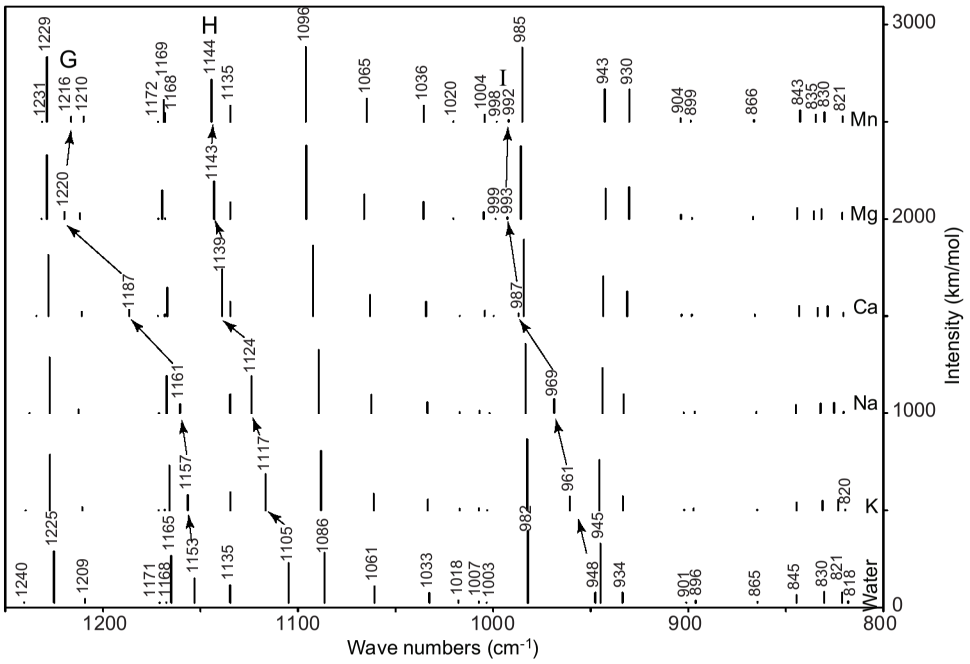

Figure 9: Calculated infrared bands of AfB_1 and AfB_1-Metal complexes in the range of 800 to 1250 cm^{-1}.